

1 Reviewer#1

2
3
4 The paper documents the methodology and results from the use of FLEXPART on
5 the IAGOS dataset, with the goal of providing potential users with source attribution.
6 The paper is well-written and provide a good description of the methodology. The
7 application portion of the paper is more limited, focusing on a few examples and broad
8 measures. Overall, I find the paper worthy of publication after consideration of the
9 following points.

10
11 We would like to thank Reviewer#1 for her/his comments and suggestions that will improve
12 our manuscript.

13 We clarified all the points raised by reviewer#1 and answered her/his different remarks in
14 blue in this document.

15
16
17 Major point

18 While there is a wealth of information provided by all the parcels released along the
19 flight track, the authors do not provide any information on the standard deviation (or any
20 other statistical information) of the simulation perturbation. In particular, this seems to
21 be of relevance to the discussion of Figure 11.

22
23 We provided statistical information in the submitted version through the percentiles
24 information given in Fig 10b which are commented in Section 5.2.

25 In addition, as suggested by Rev#1, we have added in the revised version of the manuscript
26 different statistical information.

27 SOFT-IO standard deviation has been added to Figure 11, as suggested by Rev#1, but also on
28 Figs.#5 #6 #7 and #8 (see below for the modifications).

29 Additionally, we have also added standard deviation of the IAGOS vs SOFT-IO bias on
30 Figure 10a, but not on Figs.12a and 13a for clarity reason.

31 The discussion related to the figures has been modified accordingly to take into account this
32 new information on standard deviation in Section 5.2, as suggested by Rev.#1.

33
34 Minor points

35 - Line 162: It is not clear the vertical resolution is the most critical factor. Plenty of
36 processes (as discussed in the paper) are not present in trajectories, or a choice of
37 different parameters, could also be responsible for trajectory shortcomings.

38 We have modified line 162 in order to account Ref#1 remark:

39 “ *Vertical resolution is one of the most critical factor for modeling such CO plumes with the*
40 *best precision in terms of location and intensity (Eastham and Jacob, 2017)”*

41
42 - Line 208: Why the ICARTT dataset? There are plenty of regional dataset that might
43 have been of higher relevance than this one. It would be good to justify this choice

44 Ref#1 is true that there are plenty of regional dataset that could have been tested. The goal of
45 using regional dataset in the paper is to evaluate the incidence of one of them respect to global
46 emission inventories, not to evaluate the incidence of all regional dataset. We have chosen
47 ICARTT because of improved results demonstrated in the representation of boreal biomass
48 burning fires in some specific cases (Elguindi et al., 2010; Turquety et al., 2016). Boreal fires
49 can be associated with pyro-convection, generally poorly represented in global emissions
50 inventories. As IAGOS has a quasi global coverage, global emission inventories are the first

51 choice in the methodology. However ICARTT comparison showed that regional inventories
52 could be used to obtain better results on limited case studies on CO observations related to
53 extreme events such as pyro-convection, and suggests that other regional emission inventories
54 could be then included in the future in SOFT-IO for specific case studies CO pollution.

55 We have added the following sentence lines 206-209:

56 *“The aim is to test the ability of regional inventories in better representing simulated CO for*
57 *specific case studies. The goal of using regional dataset in this paper is only to evaluate the*
58 *incidence of one of them respect to global emission inventories, not to evaluate the incidence*
59 *of all regional dataset. We have chosen ICARTT because of improved results demonstrated in*
60 *the representation of boreal biomass burning fires in some specific cases (Turquety et al.,*
61 *2016) as for example the one based on MOZAIC data by Elguindi et al., (2010). Global*
62 *emission inventories are the first choice to interpret quasi global coverage of the CO IAGOS*
63 *measurements. In the future we plan to include regional emission inventories for the study of*
64 *specific events.”*

65

66 - Line 220: it seems that the CO lifetime is not part of this equation. This would be a
67 serious issue since 20-day trajectories are considered. If used, what is the CO lifetime?

68 CO is considered as chemically passive tracer in the equation. Concentrations will only vary
69 considering dispersion and mixing associated with dynamical processes along 20 days.

70 The only significant chemical sink of CO in the troposphere is OH attack. As stated in lines
71 80-81, CO has lifetime of months in the troposphere (Logan et al., 1981; Mauzerall et al.,
72 1998), higher than the 20-day of backtrajectories. Folkins et al. (JGR 2006) calculated CO
73 lifetime against OH attacks (their Fig. 11) between 20-25 and 80 days within the troposphere,
74 confirming that trajectories lower than 20-25 days should be used to avoid chemistry issues in
75 CO lifetime.

76

77 - Line 228: it is also important to recognize the CO tends to be mostly released during
78 smoldering and so might not be as prevalent in pyrocumuli.

79 The following sentence has been added line 228:

80 *“even if CO tends to be mostly released during smoldering”*

81

82 - Line 286: it is not clear that it is always a straight linear decay with altitude. How
83 important is the definition of the background?

84 We agree that there is not always a straight linear decay of CO with altitude. However, as for
85 most of the IAGOS vertical profiles CO is enhanced in the boundary layer (related to surface
86 emissions), the calculation of the background by using the slope calculated in the free
87 troposphere was the most accurate way to define the background.

88 This definition of the background could be in the future improved by using “climatological”
89 CO vertical profiles. It will be only possible to use this with sufficient CO measurements
90 above the different IAGOS airports, and this was not possible for the present study over 10
91 years of CO measurements, except for few exceptions (Frankfurt for instance). Note that the
92 definition of the background does not enter in the SOFT-IO methodology neither in the final
93 CO ancillary data included in the IAGOS database. The background is defined in the present
94 study to extract CO anomalies in order to statistically evaluate the differences with the
95 contribution in CO computed by SOFT-IO. Finally the CO background definition has a
96 negligible incidence in the CO anomalies definition, as we focus on the anomalies higher than
97 the percentile 75 (see Eq. 4 and 5 lines 303-304)

98

99 - Line 295: is there any assurance that the background from VP is consistent with UT
100 where they connect? If not, is this an issue?

101 Two different methodologies are used to estimate the background in UT and VP, as we still
102 do not have enough data over all airports to apply climatological background for VP.
103 Background is not used to provide ancillary data of CO in the IAGOS database and its
104 definition is quite subjective (see for instance Parrish et al., 2012, doi:10.5194/acp-12-11485-
105 2012). We estimate a background in the submitted paper to evaluate SOFT-IO simulations
106 respect to CO anomalies events.
107 This is neither an issue for the provision of CO ancillary data calculated with SOFT-IO in the
108 IAGOS database, nor for the estimation of CO anomalies as we focus on events higher than
109 percentile 75, as explained just above.
110
111 - Line 301: change “to consider” to “to be considered”
112 Done
113
114 - Line 366: it would be nice to show PV along the same track
115 PV has been added in dark green along flight track on Figs.6a and 8a (see below)
116
117 - Line 425: Figure needs an explanation of the color bar labels.
118 Explanation of the color bar levels has been added (see below)
119
120 - Line 465: change “less good” to “worse”
121 Change is done line 465
122
123 - Line 471: I think it would be quite illuminating to present an additional figure (within
124 the text or in the supplement) with percentages instead of concentrations.
125 We have added additional figures of relative bias in supplement section (Figs S2a, S2b, S2c
126 and S2d)
127
128 - Line 488: this might look quite different with percentages!
129 Figures with relative bias have been added in supplement (Fig S2a, S2b, S2c and S2d)
130
131 - Line 497: this seems like a very narrow explanation.~a There are many things that
132 could go wrong, not just pyro-cumulus.
133 Rev#1 is true. We have added the following sentence line 497:
134 “, or these emission inventories are under estimated for such specific events”
135
136 - Line 502: I think “sense” is better than “information”
137 Information has been replaced by sense
138
139 - Line 508: this seems like too many plots since very little discussion is attached to
140 Them
141 Plots have been implemented over one page
142
143 - Line 513: as mentioned in my major point above, the question is but what is the range
144 of the variability from the different parcels?~a The only thing that this is showing is that
145 the mean is within the observed standard deviation.
146 As mentioned previously, we have added standard deviation into the figure and discussed it in
147 Section 5.2. We clearly see that the standard deviation of the model is within the standard
148 deviations of the observations in the LT and in the UT, but not in the MT.

149
150 - Line 549: it is hard to get a sense of the change from the Taylor diagrams. If the authors
151 want to keep them, it might be quite helpful to have arrows indicating the direction
152 of the change.

153 [We have added connection lines to help the reader interpreting the direction of change in the](#)
154 [Taylor diagrams \(see below\)](#)

155
156 - Line 555: this is actually incorrect. The anthropogenic emissions in MACCity originated
157 from Lamarque et al. (ACP, 2010), except for the added seasonal cycle. Emissions
158 were harmonized for year 2000 with the various scenarios (RCPs); therefore,
159 any data post-2000 is actually the result of the scenario RCP8.5. The fact that they are
160 fairly close is that they share many aspects (see paper above for more details).

161 “
162 [Rev#1 is true. We have updated information concerning MACCity in our manuscript in order](#)
163 [to consider this remark. The following sentences have been added:](#)

164 *“These results are not surprising as MACCity (Lamarque et al., 2010; Granier et al., 2011) is*
165 *originated from various regional inventories (in addition to EDGAR), and expect to better*
166 *represent...”*

167 *“However as stated in Lamarque et al., (2010) both inventories share many aspects (for*
168 *example over Latin and South America), and the differences between them...”*

169 Reviewer#2

170
171 This paper by Sauvage et al., presents a system (SOFT-IO) based on the extensive use
172 of FLEXPART dispersion model (coupled with different inventories of anthropogenic
173 and fire emissions), created to analyse and attribute the variability of atmospheric
174 composition observed along a huge number of observations by the IAGOS-MOZAIC
175 programme. Even if, in this current configuration, the system is able to simulate only
176 CO variability, it is valuable for the interpretation of this important long-term data base.
177 From my understanding, the SOFT-IO outputs will be easily accessible to external users
178 and thus they represent a potentially powerful tool for a number of applications. Since
179 the system is based on a pre-computed data-set of air-mass transport simulation by
180 FLEXPART model, it is possible to couple it with other emission inventories besides
181 those used in this work. As a personal comment, it would be really great if this system
182 will be made available also for other observation systems (e.g. WMO/GAW stations).
183 Other than presenting SOFT-IO tool, the paper also provides an assessment of its performance
184 in correcting reproducing the variability of observed CO due to anthropogenic
185 and fire emissions over differentWorld regions (where the IAGOS-MOZAIC programme
186 is/was active) also discussing (by mean of case study analysis, and sensitivity studies)
187 the dependency of SOFT-IO results as a function of different parameters (i.e. different
188 input meteorological data-set, different emission inventories, different scheme for pyroconvection).
189 By discussing the differences between SOFT-IO simulations and observations,
190 the paper also provides information about the accuracy of different emission
191 inventories or pyro-convection schema.
192 The paper is clear and very well written and I strongly recommend publication after
193 that some points (most of them, minor) are considered.

194
195 [We would like to thank Reviewer#2 for her/his comments and suggestions that will improve](#)
196 [our manuscript. We clarified all the points raised by reviewer#2 and answered her/his](#)
197 [different remarks or comments in blue in this document and in the revised manuscript.](#)
198

199
200
201
202
203
204
205
206
207
208
209
210
211
212
213
214
215
216
217
218
219
220
221
222
223
224
225
226
227
228
229
230
231
232
233
234
235
236
237
238
239
240
241
242
243
244
245
246
247
248
249
250

However, I have to stress (this is my only major concern) that the scientific significance of the SOFT-IO simulations are only limited discussed. As an instance, the authors provided very interesting longterm time series of CO over different regions of the World but without giving any comments or indications about differences among regions, about the existence/attribution of long-term trends (both in observations and simulations) , about seasonal variability or SOFT-IO agreement with other data-sets apart MOZAIC.

Rev#2 is true that there is limited discussion of the scientific significance of SOFT-IO simulations. This choice is deliberate. Indeed as stated in the “Introduction” section (lines 86-90 of the submitted manuscript), the goal of the paper is to present and validate SOFT-IO as well as the CO ancillary products calculated with SOFT-IO, for the IAGOS database and the IAGOS users.

Ancillary products calculated with SOFT-IO will then be implemented in the IAGOS database, so that further scientific interpretations of the IAGOS data using SOFT-IO will follow in future papers realized by IAGOS database users.

For instance, long-term CO series have been first analyzed in a recent study of Cohen et al. (2017, <https://doi.org/10.5194/acp-2017-778>). Our study just aim to evaluate SOFT-IO in terms of long-term series reproducibility (Figure 11). The use of SOFT-IO to comment the existence/attribution, or to give indication about the differences in regional trends will be done in further studies, out of the scope of this paper. However, this is definitely our objective, to go further for example regarding the CO trends analysis than the recent Cohen et al., 2017 work.

Moreover, as stated in the introduction, the main goal of SOFT-IO is to provide ancillary data that should help the IAGOS users interpreting the IAGOS database. SOFT-IO source code will be available as soon as the paper would be accepted, so that everybody could use it on other data-sets as suggested by Ref#2. We encourage external users to apply SOFT-IO to other dataset, such as ground based CO measurements, or for CO aircraft campaigns. However it is out of the scope of this study to evaluate the model to other dataset but IAGOS. Indeed IAGOS represents to our knowledge the densest in-situ measurements CO dataset, and it will be easier to apply SOFT-IO to other in situ CO datasets.

We modified the following sentence lines 86-90 for more clarity:

“The goal is to provide the scientific community with added value products that will help them analyzing and interpreting the large number of IAGOS measurements. The methodology is focused on the development of a scientific tool (SOFT-IO version 1.0) based on FLEXPART particle dispersion model, that simulates the contributions of anthropogenic and biomass burning emissions for IAGOS CO measurements. This tool, which has the benefit to be adaptable to multiple emission inventories without re-running FLEXPART simulations, is described and then evaluated in the present study with the large data-sets of IAGOS CO measurements. SOFT-IO could be in the future easily adapted and used to analyze other datasets of trace gas measurements such as from ground based observations, sondes, aircraft campaigns or satellite observations.”

In the same way, possible limitations/inaccuracy of the considered emission inventories (which have been pointed out by the authors) must be better addressed/discussed also in view of their extensive use in air-quality or climate studies.

In the same way, we deliberately did not discuss the limitations and accuracy of the emission inventories. This is out of the scope of the paper. SOFT-IO could be in a future a useful tool

251 to investigate emission inventories limitations or accuracy by the scientific community in
252 charge of developing emission inventories, or investigating air quality or climate studies. The
253 present paper only aims to present the SOFT-IO tool developed to help IAGOS users
254 interpreting a large database such as the IAGOS one, to evaluate the tool against IAGOS data.
255 Therefore, we provide these CO contributions to the IAGOS users as added-value products.

256
257 Finally, I visited the IAGOS web site but I was not able to find SOFT-IO output. Probably,
258 they are still not available to external users: : :

259 **Rev#2 is true, we believe that our validation paper should be accepted to make the code and**
260 **the data available for external users.**

261
262

263 Minor/technical points

264
265

266 1) Figure 2: it seems that for boreal fires (with FRP > 10 Tjday)
267 the injection fraction decrease with height along the first atmospheric layers (up to 2000
268 m). It is correct? This is the effect of atmospheric vertical mixing/stability?

269 **For boreal fires (> 10 and < 100TJ/day; > 100TJ/day), the injection fraction decreases with**
270 **height higher than 3000m. Indeed this is the effect of atmospheric vertical mixing, as**
271 **calculated by the PRMv2 model.**

272

273 2) In general the figure should be better arranged. I would recommend the authors to
274 reshape the plots so that each full figure (often composed by several plates) can be
275 showed in a single page. This would help the reader also in comparing the results of
276 the sensitivity tests

277 **We have arranged the figures so that they are on a single page.**

278

279 3) Table 3: please provide some statistical indications to provide quantitative indication
280 about the agreement for the two inventories (e.g. by providing average CO values for
281 observations and simulations, mean bias, timing of the detected peak, std. dev..)

282 **We have added statistical information for Table 3 and Table 4 (see below)**

283

284 4) Pag 6. To me is not clear how the injection profile is defined: : :please clarify it.

285 **The injection profile is defined according to three methodologies, as explained page 7 lines**
286 **225-252, the DENTENER, the MIXED or the APT one.**

287 **In order to clarify, we add the following sentence lines 217-218:**

288 ***“ and defined according to three different approaches (DENTENER, MIXED or APT)***
289 ***described in the next paragraph”***

290

291 5) Pag. 10. It's not clear why you claimed that only 2/3 of peaks are simulated by
292 EDGAR. In my opinion, all the peaks are simulated by EGARD run indeed

293 **All the peaks are simulated by EDGAR, but only 2/3 of the peaks intensity is reproduced**
294 **using EDGAR.**

295 **We will rephrase lines 374-375**

296 ***“Only 2/3 of the observed enhancements are simulated using EDGARv4.2, except for plume 1***
297 ***with better results” with “Using EDGARv4.2, only 2/3 of the observed CO enhancements***
298 ***intensity is reproduced, except for plume #1 with better intensity results”***

299

300 6) Fig. 11, line 413. Thus the incorrect quantification of the bottom part of the peak by
301 the ICARTT run can be attribute to not perfect transport/mixing by FLEXPART? Please
302 comment, on that.

303 **It seems that Rev#2 refers here to Fig.7a. In this case it is hard to explain why the bottom part**
304 **of the peak is not represented as well as the upper part, either by ICARTT, GFED or GFAS. It**

305 could indeed be related to transport processes in FLEXPART, but also in the ECMWF
306 analyses or in the vertical profiles injection.

307

308 7) Pag 12, Figure 9: it can be interesting also to separate the plumes attributed to fires
309 from these due to anthropogenic emissions .

310 Ideally this could be interesting. But this is not possible to realize. Indeed all the plumes are
311 influenced both by biomass burning and anthropogenic emissions, as we can see on the case
312 studies displayed on Figures 5 to 8. In order to do that we should define subjective criteria to
313 attribute a plume to either biomass burning or anthropogenic emissions. This is out of the
314 scope of this study.

315

316 8) Pag 13, line 493: I would say that for North Asia UT discrepancies varied from -100
317 to + 200 ppb and for South Asia LT from - 50 to +100 ppb.

318 We have modified line 493 with Rev#2 suggestion:

319 *“North Asia UT discrepancies varies from -100 ppb to +200 ppb and from -50 ppb to +100*
320 *ppb for South Asia LT. “*

321

322 9) Pag 14, line 516: the possible misrepresentation of anthropogenic emissions after
323 2009 is a point of great importance that deserve more discussion. The overestimation
324 in the MT appeared to be more and more relevant over NAM than EU. Please comment.

325 Rev#2 is true. As stated in Stein et al., 2004, the largest near-surface CO bias are found over
326 Europe in January.

327 We have added the following lines 519:

328 *“This suggests misrepresentation of anthropogenic emissions in Europe after the year 2009.*
329 *Indeed Stein et al., (2014) suggested the lower near-surface CO bias was found in Europe in*
330 *relation with possible under estimation of traffic emissions in the inventories.”*

331

332 It is also true that the overestimation in the MT appears higher over NAM rather than over
333 EU. This could be related to two causes:

- 334 • Less measurements in the MT over NAM than over EU
- 335 • Greater proximity of the NAM MT to summer sources, such as boreal fires, that could
336 explain the higher overestimation particularly in this season.

337

338 We add the following lines 519-529

339 *“In the middle troposphere (2-8 km), the CO plumes are systematically overestimated by*
340 *SOFT-IO by 50% to 100% compared to the observations, with larger standard deviation and*
341 *higher overestimation over NAM. This might be related to different reasons:*

- 342 • *the chosen methodology of the CO plume enhancements detection for those altitudes*
343 *(described in Sect. 3.4), which may lead to a large number of plumes with small CO*
344 *enhancements, which are difficult to simulate. This could be due to the difficulty in*
345 *defining a realistic CO background in the middle troposphere.*
- 346 • *the source-receptor transport which may be more difficult to simulate between 2-8 km*
347 *than in the LT where receptors are close to sources; or than in the UT where most of*
348 *the plumes are related to convection detrainment better represented in the models*
349 *than MT detrainment which might be less intense.*

- 350 • *The frequency of the IAGOS observations which is lower in the LT and in the MT than*
351 *in the UT.*
- 352 • *Higher overestimation over NAm MT than Eur MT could be first related to lower*
353 *frequency of measurements in the NAm. Moreover overestimation is greater during*
354 *summer when NAm MT is closer to summer sources such as boreal fires, while Eur*
355 *MT is related to CO air masses more diluted with background air during transatlantic*
356 *transport. ”*

357

358 10) Pag 15, line 559: I would not say that EDGAR performed better than MACC inventory

359 for CAS_MT and NAS_UT: are these differences really significant?

360 *Indeed results are better using EDGAR for specific regions. Ref#2 is right. Differences are*
361 *not statistically significant for NAs_UT, but they are for CAs_MT (almost 50% difference*
362 *between the two simulations with the two inventories).*

363 *We rephrase line 559 with the following “Regionally, however, results with EDGARv4.2 can*

364 *be better by almost 50%, such as over South Asia LT and MT, Central Asia LT and MT”*

365

366

367

368

369

370

371

372

373

374

375

376

377

378

379

380

381

382

383

384

385 **Marked-up manuscript version:**

386

387

388

389

390 **Source attribution using FLEXPART and carbon monoxide**
391 **emission inventories: SOFT-IO version 1.0**

392 Bastien Sauvage¹, Alain Fontaine¹, Sabine Eckhardt³, Antoine Auby⁴, Damien Boulanger²,
393 Hervé Petetin¹, Ronan Paugam⁵, Gilles Athier¹, Jean-Marc Cousin¹, Sabine Darras³, Philippe
394 Nédélec¹, Andreas Stohl³, Solène Turquety⁶, Jean-Pierre Cammas⁷ and Valérie Thouret¹.

395

396 ¹Laboratoire d'Aérodynamique, Université de Toulouse, CNRS, UPS, France

397 ²Observatoire Midi-Pyrénées, Toulouse, France

398 ³NILU - Norwegian Institute for Air Research, Kjeller, Norway

399 ⁴CAP HPI, Leeds, United Kingdom

400 ⁵King's College, London, United Kingdom

401 ⁶Laboratoire de Météorologie Dynamique/IPSL, UPMC Univ. Paris 6, Paris, France

402 ⁷Observatoire des Sciences de l'Univers de la Réunion (UMS 3365) et Laboratoire de l'Atmosphère et des
403 Cyclones (UMR 8105), Université de la Réunion, Saint-Denis, La Réunion, France

404

405

406 *Correspondence to:* Bastien Sauvage (bastien.sauvage@aero.obs-mip.fr)

407 **Abstract.** Since 1994, the In-service Aircraft for a Global Observing System (IAGOS) program has produced
408 in-situ measurements of the atmospheric composition during more than 51000 commercial flights. In order to
409 help analyzing these observations and understanding the processes driving the observed concentration
410 distribution and variability, we developed the SOFT-IO tool to quantify source/receptor links for all measured
411 data. Based on the FLEXPART particle dispersion model (Stohl et al., 2005), SOFT-IO simulates the
412 contributions of anthropogenic and biomass burning emissions from the ECCAD emission inventory database
413 for all locations and times corresponding to the measured carbon monoxide mixing ratios along each IAGOS
414 flight. Contributions are simulated from emissions occurring during the last 20 days before an observation,
415 separating individual contributions from the different source regions. The main goal is to supply added-value
416 products to the IAGOS database by evincing the geographical origin and emission sources driving the CO
417 enhancements observed in the troposphere and lower stratosphere. This requires a good match between observed
418 and modeled CO enhancements. Indeed, SOFT-IO detects more than 95% of the observed CO anomalies over
419 most of the regions sampled by IAGOS in the troposphere. In the majority of cases, SOFT-IO simulates CO
420 pollution plumes with biases lower than 10-15 ppbv. Differences between the model and observations are larger
421 for very low or very high observed CO values. The added-value products will help in the understanding of the
422 trace-gas distribution and seasonal variability. They are available in the IAGOS data base via
423 <http://www.iagos.org>. The SOFT-IO tool could also be applied to similar data sets of CO observations (e.g.

424 ground-based measurements, satellite observations). SOFT-IO could also be used for statistical validation as well
425 as for inter-comparisons of emission inventories using large amounts of data.

426 **1 Introduction**

427 Tropospheric pollution is a global problem caused mainly by natural or human-triggered biomass burning,
428 and anthropogenic emissions related to fossil fuel extraction and burning. Pollution plumes can be transported
429 quickly on a hemispheric scale (within at least 15 days) by large scale winds or, more slowly (Jacob, 1999),
430 between the two hemispheres (requiring more than 3 months). Global anthropogenic emissions are for some
431 species (CO₂) in constant increase (Boden et al., 2015). However, recent commitments of some countries to
432 reduce greenhouse gas emissions (e.g. over the U.S., U.S. EPA's Inventory of U.S. Greenhouse Gas Emissions
433 and Sinks, 1990-2013; <http://www.epa.gov/climatechange/ghgemissions/usinventoryreport.html>) seems to
434 induce a stalling in other global emissions (NO_x, SO₂ and Black Carbon, Stohl et al., 2015), except for some
435 regions (Brazil, Middle East India, China) where NO_x emissions increase (Miyazaki, 2017). In order to better
436 understand large-scale pollution transport, large amounts of in situ and space-based data have been collected in
437 the last three decades, allowing a better understanding of pollution variability and its connection with
438 atmospheric transport patterns (e.g. Liu et al., 2013). These data-sets are also useful to quantify global pollution
439 evolution with respect to the emissions trends described above.

440 Despite the availability of large trace gas data sets, the data interpretation remains difficult for the following
441 reasons: (1) the sampling mode does not correspond to an a priori defined scientific strategy, as opposed to data
442 collected during field campaigns; (2) the statistical analysis of the data can be complicated by the large number
443 of different sources contributing to the measured pollution, and an automated analysis of the contributions from
444 these different sources is required if, for instance, regional trends in emissions are to be investigated; (3) the
445 sheer size of some of the data sets can make the analysis rather challenging. Among the long-term pollution
446 measurement programs, the IAGOS airborne program (<http://www.iagos.org/>, formerly known as the
447 Measurement of OZone by Airbus In-service airCRAFT -MOZAIC- program) is the only one delivering in-situ
448 measurement data from the free troposphere. IAGOS provides regular global measurements of ozone (O₃) - since
449 1994 -, carbon monoxide (CO) - since 2002 -, and nitrogen oxides (NO_y) – for the period 2001-2005 - obtained
450 during more than 51000 commercial aircraft flights up to now, with substantial extent of the instrumented
451 aircraft recently. The analysis of the IAGOS database is also complicated by the fact that primary pollutants (CO
452 and part of NO_y) are emitted by multiple sources, while secondary compounds (O₃) are produced by
453 photochemical transformations of these pollutants, often most efficiently when pollutants from different sources
454 mix.

455 A common approach to separate the different sources influencing trace gas observations is based on the
456 determination of the air mass origins through Lagrangian modeling. This approach allows linking the emission
457 sources to the trace gas observations (e.g. Nédélec et al., 2005; Sauvage et al., 2005, 2006; Tressol et al. 2008;
458 Gressent et al. 2014; Clark et al., 2015; Yamasoe et al., 2015). Lagrangian modeling of the dispersion of
459 particles allows accounting efficiently for processes such as large-scale transport, turbulence and convection.
460 When coupled with emission inventories Lagrangian modeling of passive tracers allows for instance to
461 understand ozone anomalies (Cooper et al., 2006; Wen et al., 2012), to quantify the importance of lightning NO_x
462 emissions for tropospheric NO₂ columns measured from space (Beirle et al., 2006), to investigate the origins of

463 O₃ and CO over China (Ding et al., 2013), or to investigate the sources influencing the observed CO₂ over the
464 high northern latitudes (Vay et al., 2011).

465 To help analyzing a large data set such as the IAGOS observations, it is important to provide scientific users
466 a tool for characterizing air mass transport and emission sources. This study presents a methodology to
467 systematically establish a link between emissions sources (biomass burning and anthropogenic emissions) and
468 concentrations at the receptor locations. Since CO is a substance that is emitted by combustion sources (both
469 anthropogenic and biomass burning) and since CO has a lifetime of months in the troposphere (Logan et al.,
470 1981; Mauzerall et al., 1998), it is often used as a tracer for pollution transport (Staudt et al. 2001; Yashiro et al.,
471 2009; Barret et al., 2016). It is therefore convenient to follow past examples and use simulated CO source
472 contributions to gauge the influence of pollution sources on the measurements also with SOFT-IO. Our
473 methodology uses the FLEXPART Lagrangian particle dispersion model (Stohl et al., 2005) and emission
474 inventories from the ECCAD emission database (Granier et al., 2012) in order to quantify the influence of
475 emissions sources on the IAGOS CO measurements. The goal is to provide the scientific community with added
476 value products that will help them analyzing and interpreting the large number of IAGOS measurements. The
477 methodology [is focused on the development of a scientific tool \(SOFT-IO version 1.0\) based on FLEXPART](#)
478 [particle dispersion model, that simulates the contributions of anthropogenic and biomass burning emissions for](#)
479 [IAGOS CO measurements. This tool, which](#) has the benefit to be adaptable to multiple emission inventories
480 without re-running FLEXPART simulations, [is described and then evaluated in the present study with the large](#)
481 [data-sets of IAGOS CO measurements. SOFT-IO could be in the future](#) easily adapted and used to analyze other
482 datasets of trace gas measurements such as from ground based observations, sondes, aircraft campaigns or
483 satellite observations.

484 The methodology will be described in the next section, and then evaluated at the example of case studies of
485 pollution plumes observed by IAGOS aircraft. Further evaluation is performed through statistical analysis.
486 Finally we discuss the limitations of the methodology by estimating its sensitivity to different input data sets
487 (emission inventories, meteorological analyses).

488 **2. In-situ observations database: MOZAIC and IAGOS programs**

489 The MOZAIC program (Marenco et al., 1998) was initiated in 1993 by European scientists, aircraft
490 manufacturers and airlines to better understand the natural variability of the chemical composition of the
491 atmosphere and how it is changing under the influence of human activity, with particular interest in the impact of
492 aircraft exhaust. Between August 1994 and November 2014, MOZAIC performed airborne in-situ measurements
493 of ozone, water vapor, carbon monoxide, and total nitrogen oxides. The measurements are geolocated (latitude,
494 longitude and pressure) and come along with meteorological observations (wind direction and speed,
495 temperature). Data acquisition is performed automatically during round-trip international flights (ascent, descent
496 and cruise phases) from Europe to America, Africa, Middle East, and Asia (Fig. 1).

497 Based on the technical expertise of MOZAIC, the IAGOS program (Petzold et al., 2015, and references therein)
498 has taken over and provides observations since July 2011. The IAGOS data set still includes ozone, water vapor,
499 carbon monoxide, meteorological observations, and measurements of cloud droplets (number and size) are also
500 performed. Depending on optional additional instrumentation, measurements of nitrogen oxides, total nitrogen
501 oxides or, in the near-future, greenhouse gases (CO₂ and CH₄), or aerosols, will also be made.

502 Since 1994, the IAGOS-MOZAIC observations have created a big data set that is stored in a single database
503 holding data from more than 51000 flights. The data set can be used by the entire scientific community, allowing
504 studies of chemical and physical processes in the atmosphere, or validation of global chemistry transport models
505 and satellite retrievals. Most of the measurements have been collected in the upper troposphere and lower
506 stratosphere, between 9 and 12 km altitude, with 500 flights/ aircraft/ year on up to 7 aircraft up to now.

507

508 The MOZAIC and IAGOS data (called “IAGOS” from here on) used in this study are in-situ observations of CO
509 only, which is being measured regularly on every aircraft since 2002 with more than 30000 flights, using a
510 modified infrared filter correlation monitor (Nédélec et al., 2003; Nédélec et al., 2015). The accuracy of the CO
511 measurements has been estimated at (30 s response time) ± 5 ppb, or $\pm 5\%$.

512

513 Several case studies of CO pollution plumes (Table 1) using IAGOS data have been published, where model
514 simulations allowed attribution of the measured CO enhancements to anthropogenic or biomass burning
515 emissions, either measured in the boundary layer or in the free troposphere, following regional or synoptic-scale
516 transport (e.g. Nédélec et al., 2005; Tressol et al., 2008; Cammas et al., 2009; Elguindi et al., 2010). These case
517 studies are used here to better define the requirements for our methodology (meteorological analyses and
518 emission inventory inputs). Some of them are detailed and re-analyzed in Sect. 4.

519 **3. Estimation of carbon monoxide source regions: methodology**

520 To establish systematic source-receptor relationships for IAGOS observations of CO, the Lagrangian dispersion
521 model FLEXPART (Stohl et al., 1998, 2005; Stohl and Thomson, 1999) is run over the entire database.
522 Lagrangian dispersion models usually represent the differential advection better than global Eulerian models
523 (which do not well resolve intercontinental pollution transport; Eastham et al., 2017), at a significantly lower
524 computational cost. In particular, small-scale structures in the atmospheric composition can often be
525 reconstructed from large-scale global meteorological data, which makes model results comparable to high-
526 resolution in situ observations (Pisso et al., 2010). In the past, many studies (Nédélec et al., 2005 ; Tressol et
527 al.,2008; Cammas et al., 2009; Elguindi et al., 2010; Gressent et al., 2014) used FLEXPART to investigate
528 specific pollution events observed by the IAGOS aircraft. However, in these former case studies, the link
529 between sources and observations of pollution was guessed a priori. The transport model was then used to
530 validate the hypothesis. For example, in the Cammas et al. (2009) study, observations of high CO during summer
531 in the upper troposphere and lower stratosphere east of Canada were guessed to originate from biomass burning
532 over Canada as this region is often associated with pyro-convection whose intensity usually peaks in the
533 summer. This origin was confirmed by the model analysis. In general, the origin of the observed pollution cannot
534 be guessed a priori, especially when analyzing measurements from thousands of flights. Moreover, multiple
535 sources are most of the time involved when the observed pollution is the result of the mixing of polluted air
536 masses from different regions and source types.

537 CO is often used as a tracer to quantify the contributions of the different sources to the observed pollution
538 episodes. CO is emitted by both the combustion of fossil fuels and by biomass burning, and its photochemical
539 lifetime against OH attack is usually 1 to 2 months in the troposphere (Logan et al., 1981; Mauzerall et al.,

540 1998). Therefore it is possible to link elevated CO mixing ratios (with respect to its seasonally varying
541 hemispheric baseline) to pollution sources without simulating the atmospheric chemistry.

542 **3.1 Backward transport modeling**

543 Simulations were performed using the version 9 of FLEXPART, which is described in detail by Stohl et al.
544 (2005) (and references therein). The model was driven using wind fields from the European Centre for Medium-
545 Range Weather Forecast (ECMWF) 6-hourly operational analyses and 3-hour forecasts. The ECMWF data are
546 gridded with a $1^\circ \times 1^\circ$ horizontal resolution, and with a number of vertical levels increasing from 60 in 2002 to
547 137 since 2013. The model was also tested using higher horizontal resolution (0.5°), and with ECMWF ERA-
548 Interim reanalysis, as their horizontal and vertical resolution and model physics are homogeneous during the
549 whole period of IAGOS CO measurements. However, operational analyses were used for our standard set-up, as
550 the transport model reproduced CO better when using these data for several case studies of pollution transport,
551 especially for plumes located in the UT. Indeed, operational analyses provide a better vertical resolution since
552 2006 (91 levels until 2013, then 137 levels against 60 levels for ERA-Interim) and thus a better representation of
553 the vertical wind shear, and the underlying meteorological model is also more modern than the one used for
554 producing ERA-Interim. Vertical resolution is one of the critical factors for modeling such CO plumes with the
555 best precision in terms of location and intensity (Eastham and Jacob, 2017).

556 Using higher horizontal resolution for met-fields analyses and forecasts (0.5° vs 1°) showed no influence on the
557 simulated carbon monoxide, despite larger computational time and storage needs. We assume further
558 improvement can be obtained using even higher horizontal resolution (0.1°), but this was not feasible at this
559 stage and should be considered in the future.

560

561 In order to be able to represent the small-scale structures created by the wind shear and observed in many
562 IAGOS vertical profiles, the model is initialized along IAGOS flight tracks every 10 hPa during ascents and
563 descents, and every 0.5° in latitude and longitude at cruise altitude. This procedure leads to i model initialization
564 boxes along every flight track. For each i , 1000 particles are released. Indeed 1000 to 6000 particles are
565 suggested for correct simulations in similar studies based on sensitivity tests on particles number (Wen et al.,
566 2012; Ding et al., 2013). For instance, a Frankfurt (Germany) to Windhoek (Namibia) flight contains around 290
567 boxes (290000 particles) of initialization as a whole.

568 FLEXPART is set up for backward simulations (Seibert and Frank, 2004) from these boxes as described in Stohl
569 et al. (2003) and backward transport is computed for 20 days prior to the in-situ observation, which is sufficient
570 to consider hemispheric scale pollution transport in the mid-latitudes (Damoah et al., 2004; Stohl et al., 2002;
571 Cristofanelli et al., 2013). This duration is also expected to be longer than the usual lifetime of polluted plumes
572 in the free troposphere, i.e. the time when the concentration of pollutants in plumes is significantly larger than
573 the surrounding background. Indeed, the tropospheric mixing time scale has been estimated to be typically
574 shorter than 10 days (Good et al., 2003; Pisso et al., 2009). Therefore the model is expected to be able to link air
575 mass anomalies such as strong enhancements in CO to the source regions of emissions (Stohl et al., 2003). It is
576 important to note that we aim to simulate recent events of pollution explaining CO enhancements over the
577 background, but not to simulate the CO background which results from aged and well-mixed emissions.

578 The FLEXPART output is a residence time, as presented and discussed in Stohl et al. (2003). These data
579 represent the average time spent by the transported air masses in a grid cell, divided by the air density, and are
580 proportional to the sensitivity of the receptor mixing ratio to surface emissions. In our case, it is calculated for
581 every input point along the flight track, every day for $N_t = 20$ days backward in time, on a 1° longitude x 1°
582 latitude global grid with $N_z = 12$ vertical levels (every 1 km from 0 to 12 km, and 1 layer above 12 km).
583 Furthermore, the altitude of the 2 PVU potential vorticity level above or below the flight track is extracted from
584 the wind and temperature fields, in order to locate the CO observations above or below the dynamical tropopause
585 according to the approach of Thouret et al. (2006).

586 **3.2 Emission inventories from the ECCAD project**

587 The main goal of the Emissions of atmospheric Compounds & Compilation of Ancillary Data (ECCAD) project
588 (Granier et al., 2012) is to provide scientific and policy users with datasets of surface emissions of atmospheric
589 compounds and ancillary data, i.e. data required for estimating or quantifying surface emissions. All the emission
590 inventories and ancillary data provided by ECCAD are published in the scientific literature.

591 For the current study, we selected five CO emission inventories. Four of them are available at global scale
592 (MACCity and EDGAR v4.2 for anthropogenic; GFED 4 and GFAS v1.2 -GFAS v1.0 for 2002- for fires) from
593 the ECCAD database and cover most of the IAGOS CO database presented here (2002 - 2013). The global scale
594 inventories have a $0.1^\circ \times 0.1^\circ$ to $0.5^\circ \times 0.5^\circ$ horizontal resolution. They are provided with daily, monthly or
595 yearly time resolution. They are listed in Table 2 along with the references describing them. The four global
596 inventories are used to study the model's performance and sensitivity in Sect. 5.

597 To further test the sensitivity to the emission inventories, we also used one regional inventory, which is expected
598 to provide a better representation of emissions in its region of interest than generic global inventories. [The aim is
599 to test the ability of regional inventories in better representing simulated CO for specific case studies. The goal
600 of using regional dataset in this paper is only to evaluate the incidence of one of them respect to global emission
601 inventories, not to evaluate the incidence of all regional dataset. We have chosen ICARTT because of improved
602 results demonstrated in the representation of boreal biomass burning fires in some specific cases \(Turquety et al.,
603 2016\) as for example the one based on MOZAIC data by Elguindi et al., \(2010\). Global emission inventories are
604 the first choice to interpret quasi global coverage of the CO IAGOS measurements. In the future we plan to
605 include regional emission inventories for the study of specific events.](#) For biomass burning, the International
606 Consortium for Atmospheric Research on Transport and Transformation (ICARTT) campaign's North American
607 emissions inventory developed by Turquety et al. (2007) for the summer of 2004 and provided at $1^\circ \times 1^\circ$
608 horizontal resolution was tested. It combines daily area burned data from forest services with the satellite data
609 used by global inventories, and uses a specific vegetation database, including burning of peat lands which
610 represent a significant contribution to the total emissions.

611 **3.3 Coupling transport output with CO emissions**

612 Calculating the recent contributions $C(i)$ (kg m^{-3}) of CO emissions for every one of the i model's initialization
613 points along the flight tracks requires three kinds of data:

- 614 • the residence time T_R (in seconds, gridded with $N_x = 360$ by $N_y = 180$ horizontal points, $N_z = 12$ vertical
615 levels, $N_t = 20$ days) from backward transport described in Sect. 3.1,

- CO surface emissions $E_{CO}(N_x, N_y, N_t)$ (in kg CO / m² / s)
- the injection profile $Inj(z)$ defining the fraction of pollutants diluted in the different vertical levels (with Δz being the thickness, in meters) just after emissions, and defined according to three different approaches (DENTENER, MIXED or APT) described in the next paragraph:

$$(Eq. 1) \quad C(i) = \sum_{t=1}^{N_t} \sum_{y=1}^{N_y} \sum_{x=1}^{N_x} \sum_{z=1}^{N_z} Inj(z) \frac{T_R(x, y, z, t, i) E_{CO}(x, y, t)}{\Delta z(z)}$$

In the case of anthropogenic emissions, CO is simply emitted into the first vertical layer of the residence time grid ($\Delta z = 1000\text{m}$).

For biomass burning emissions, in the tropics and mid latitudes regions, the lifting of biomass burning plumes is usually due to small and large scale dynamical processes, such as turbulence in the boundary layer, deep convection and frontal systems, which are usually represented by global meteorological models. At higher latitudes, however, boreal fires can also be associated with pyro-convection and quick injection above the planetary boundary layer, even if CO tends to be mostly released during smoldering. Pyro-convection plume dynamics are often associated with small-scale processes that are not represented in global meteorological data and emission inventories (Paugam et al 2016). In order to characterize the effect of these processes, we implemented three methodologies to parameterize biomass injection height:

- the first one (named DENTENER) depends only on the latitude and uses constant homogeneous injection profiles as defined by Dentener et al. (2006), i.e. 0-1 km for the tropics [30S-30N] (see green line in Fig 2), 0-2 km for the mid-latitudes [60S-30S, 30N-60N] (see blue line in Fig. 2) and 0-6 km for the boreal regions [90S-60S, 60N-90N] (not shown in Fig. 2).
- the second named MIXED uses the same injection profiles as in DENTENER for the tropics and mid-latitudes, but for the boreal forest, injection profiles are deduced from a lookup table computed with the plume rise model PRMv2 presented in Paugam et al. (2015). Using PRMv2 runs for all fires from different years of the Northern-American MODIS archive, three daily Fire Radiative Power (FRP) classes (under 10 TJ/day, between 10 and 100 TJ/day, and over 100 TJ/day) were used to identify three distinct injection height profiles (see brown, red, and black lines in Fig. 2). Although PRMv2 reflects both effects of the fire intensity through the input of FRP and active fire size and effects of the local atmospheric profile, here for sake of simplicity only FRP is used to classify the injection profile. Furthermore, when applied to the IAGOS data set, the MIXED method uses equivalent daily FRP estimated from the emitted CO fluxes given by the emission inventories as described in Kaiser et al. (2012)
- the third method named hereafter APT uses homogeneous profile defined by the daily plume top altitude as estimated for each 0.1x0.1 pixel of the GFAS v1.2 inventory available for 2003 to 2013 (Rémy et al. 2016, and http://www.gmes-atmosphere.eu/oper_info/global_nrt_data_access/gfas_ftp/). As in the MIXED method, GFAS v1.2 is using the plume model PRMV2 from Paugam et al. (2015), but here the model is run globally for every assimilated GFAS-FRP pixel.

654

655 3.4 Automatic detection of CO anomalies

656 For individual measurement cases, plumes of pollution can most of the time be identified by the human eye
657 using the observed CO mixing ratio time series or the CO vertical profiles. However, this is not feasible for a
658 database of tens of thousands of observation flights. In order to create statistics of the model's performance, we
659 need to systematically identify observed pollution plumes in the IAGOS database. The methodology to do this is
660 based on what has been previously done for the detection of layers in the MOZAIC database (Newell et al.,
661 1999; Thouret et al., 2000), along with more recent calculations of the CO background and CO percentiles define
662 for different regions along the IAGOS data set (Gressent et al., 2014). An example demonstrating the procedure,
663 which is described below, is shown in Fig. 3.

664

665 In a first step, the measurement time series along the flight track (number of measurements n_{TOT}) is separated
666 into three parts:

- 667 1. Ascent and descent vertical profiles (n_{VP}) in the PBL (altitudes ranging from the ground to 2 km) and in
668 the free troposphere (from 2 km to the top altitude of the vertical profiles),
- 669 2. measurements at cruising altitude in the upper troposphere (n_{UT}),
- 670 3. measurements in the lower stratosphere (n_{LS})

671 such that

$$n_{TOT} = n_{VP} + n_{UT} + n_{LS}$$

672 where n_{VP} , n_{UT} and n_{LS} are the number of measurements along tropospheric ascents and descents, and in the upper
673 troposphere and lower stratosphere, respectively. A range of altitudes from the surface to a top altitude identifies
674 vertical profiles. The top altitude is 75 hPa above the 2 pvu dynamical tropopause (Thouret et al., 2006) when
675 the aircraft reaches/leaves cruising altitude (during ascent/descent). The PV is taken from the ECMWF
676 operational analyses and evaluated at the aircraft position by FLEXPART. Observations made during the cruise
677 phase are flagged as upper tropospheric if the aircraft is below the 2 pvu dynamical tropopause. If not,
678 observations are considered as stratospheric and then are ignored in the rest of the paper. Although CO
679 contributions are calculated also in the stratosphere, the present study focuses on tropospheric pollution only.

680

681 In a second step, the CO background mixing ratio is determined for each tropospheric part (C_{VP_back} and C_{UT_back} ,
682 see Fig. 3 for illustration) for the tropospheric vertical profiles and for the upper troposphere respectively. For
683 tropospheric vertical profiles, the linear regression of CO mixing ratio versus altitude is calculated from 2 km to
684 the top of the vertical profiles, to account for the usual decrease of background CO with altitude. Data below
685 2 km are not used because high CO mixing ratios caused by fresh emissions are usually observed close to surface
686 over continents. The slope a (in ppb m^{-1}) of the linear regression is used to determine the background so that
687 $C_{VP_back} = aZ$. The background is removed from the C_{VP} tropospheric vertical profiles mixing ratio to obtain a
688 residual CO mixing ratio C_{VP}^R (Eq. 2).

$$(Eq. 2): C_{VP}^R = C_{VP} - C_{VP_back} ,$$

689

691 For the upper troposphere, the CO background mixing ratio (C_{UT_back}) is determined using seasonal median
692 values (over the entire IAGOS database) for the different regions of Figure 4. Note that this approach was not

693 feasible for vertical profiles as for most of the visited airports there are not enough data to establish seasonal
 694 vertical profiles. As for the profiles, background values are subtracted from the UT data to obtain residual C_{UT}^R
 695 (Eq. 3):

$$696 \quad (\text{Eq. 3): } C_{UT}^R = C_{UT} - C_{UT_back}$$

697

698 In a third step, CO anomalies C^A are determined for tropospheric vertical profiles (C_{VP}^A) and in the upper
 699 troposphere (C_{UT}^A). Residual C_{VP}^R and C_{UT}^R values are flagged as CO anomalies when these values exceed the
 700 third quartile (Q3) of the residual mixing ratio $C_{VP}^R(Q3)$ for vertical profiles, or the third quartile of the residual
 701 seasonal values $C_{UT_season}^R(Q3)$ in the different regions (Fig. 4) for the UT. Note that $C_{VP}^R(Q3)$ or $C_{UT_season}^R(Q3)$
 702 needs to be higher than 5 ppb (the accuracy of the CO instrument; Nédélec et al., 2015) in order to consider an
 703 anomaly:

$$704 \quad (\text{Eq. 4): } C_{VP}^A = C_{VP}^R \text{ if } C_{VP}^R > C_{VP}^R(Q3)$$

$$705 \quad (\text{Eq. 5): } C_{UT}^A = C_{UT}^R \text{ if } C_{UT}^R > C_{UT_season}^R(Q3)$$

706 In the examples shown in Fig. 3a and Fig. 3b, the red line represents CO anomalies.

707 With this algorithm CO plumes are automatically detected in the entire IAGOS database. For each identified
 708 plume, minimum and maximum values of the date, latitude, longitude and altitude, as well as the CO mean and
 709 maximum mixing ratio, are archived. These values are used for comparison with modeled CO values.

710

711 **4. Selected case studies to evaluate CO emission inventories and SOFT-IO's performance**

712 As described in Sect. 2, a number of case studies documented in the literature were selected from the IAGOS
 713 database in order to get a first impression of the model's performance. These case studies have been chosen to
 714 represent the different pollution situations that are often encountered in the troposphere in terms of emissions
 715 (anthropogenic or biomass burning) and transport (at regional or synoptic scale, pyro-convection, deep
 716 convection, frontal systems). Systematic evaluation of the model performance against emission inventories will
 717 be presented in Sect. 5.

718 **4.1 Anthropogenic emission inventories**

719 Among the case studies listed in Table 1, four were selected in order to illustrate the evaluation of the inventories
 720 used for anthropogenic emissions:

- 721 • Landing profiles over Hong Kong from 19th of July and 22nd of October 2005 were selected in order to
 722 investigate specifically Asian anthropogenic emissions.
- 723 • During the 10th of March 2002 Frankfurt–Denver and 27th of November 2002 Dallas–Frankfurt flights,
 724 IAGOS instruments observed enhanced CO plumes in the North Atlantic upper troposphere, also linked
 725 to anthropogenic emissions.

726 Figure 5a shows the observed (black line) and simulated (colored lines) CO mixing ratios above Hong Kong
 727 during 22nd of October 2005. Note that background is not simulated but estimated from the observations as
 728 described in Sect.3.4 (blue line, C_{VP_back}). The dashed blue line represents the residual CO mixing ratio C_{VP}^R .
 729 Observations show little variability in the free troposphere down to around 3 km. Strong pollution is observed

730 below, with + 300 ppb enhancement over the background on average between 0 and 3 km. Note that we do not
731 discuss CO enhancement above 3 km.

732 In agreement with C_{VP}^R , SOFT-IO simulates a strong CO enhancement in the lowest 3 km of the profile, caused
733 by fresh emissions. However, the simulated enhancement is less strong than the observed one, a feature that is
734 typical for this region, as we shall see later.

735 In addition to the CO mixing ratio, SOFT-IO calculates CO source contributions and geographical origins of the
736 modeled CO, respectively displayed in Fig. 5b and Fig. 5c (using the methodology described in Sec. 3.4) and
737 using here MACCity and GFAS v1.2 as example. For the geographical origin we use the same 14 regions as
738 defined for the GFED emissions (<http://www.globalfiredata.org/data.html>). Note that only the average of the
739 calculated CO is displayed for each anomaly (0-3km; 3.5-6km) in Fig. 5b and Fig. 5c.

740
741 Colored lines in Fig. 5a show the calculated CO using anthropogenic sources described by the two inventories
742 selected in Sect. 3.2, MACCity (green line) and EDGARv4.2 (yellow line), along the flight track. In both cases,
743 biomass burning emissions are described by GFASv1.2. Emissions from fires have negligible influence (less
744 than 3%) on this pollution event as depicted in Fig. 5b.

745 In the two simulations, the calculated CO mixing ratio is below 50 ppb in the free troposphere, as we do not
746 simulate background concentrations with SOFT-IO. CO enhancement around 4 to 6 km is overestimated by
747 SOFT-IO. CO above 6 km is not considered as an anomaly, as $C_{UT}^R < C_{UT_season}^R(Q3)$. Simulated mixing ratios in
748 the 0-2 km polluted layer are almost homogeneous, with values around 280 ppb using MACCity and around 160
749 ppb using EDGARv4.2. They are attributed to anthropogenic emissions (more than 97% of the simulated CO)
750 originating mostly from Central Asia with around 95% influence. In this regard, the CO simulated using
751 MACCity is in better agreement with the observed CO than the one obtained using EDGARv4.2. Indeed, using
752 MACCity, simulated CO reaches 90% of the observed enhancement (+ 300 ppb on average) over the background
753 (around 100 ppb), while for EDGARv4.2 the corresponding value is only 53%, indicating strong underestimation
754 of this event. The difference in the calculated CO using these two inventories is also consistent with the results
755 of Granier et al. (2011) who showed strong discrepancies in the Asian anthropogenic emissions in different
756 inventories.

757
758 Figure 6a shows the CO measurements at cruising altitude during a transatlantic flight between Frankfurt and
759 Denver on 10th of March 2002. The dashed blue line represents the residual CO C_{UT}^R . Observations indicate that
760 the aircraft encountered several polluted air masses with CO mixing ratios above 110 to 120 ppb, which are the
761 seasonal median CO values in the two regions visited by the aircraft, obtained from the IAGOS database (see
762 Gressent et al., 2014). Three pollution plumes are measured:

- 763 • around 100°W (around +10 ppb of CO enhancement on average): plume 1
- 764 • between 80°W and 50°W (+30 ppb of CO enhancement on average): plume 2
- 765 • between 0° and 10°E (+40 ppb of CO enhancement on average): plume 3.

766 These polluted air masses are surrounded by stratospheric air masses with CO values lower than 80-90 ppb. As
767 polluted air masses were sampled at an altitude of around 10 km, they are expected to be due to long-range
768 transport of pollutants.

769 The calculated CO is shown in Fig. 6a using MACCity (green line), EDGARv4.2 (yellow line) for anthropogenic
770 emissions and GFASv1.0 for biomass burning emissions. SOFT-IO estimates that these plumes are mostly
771 anthropogenic (representing 77% to 93% of the total simulated CO, Fig. 6b). Pollution mostly originates from
772 Central and South-East Asia, with strong contribution from North America (Fig. 6c) for plume 3.
773 SOFT-IO correctly locates the three observed polluted air masses with the two anthropogenic inventories. CO is
774 also correctly calculated using MACCity, with almost the same mixing ratios on average as the observed
775 enhancements in the three plumes. Using EDGARv4.2, only 2/3 of the observed CO enhancements intensity is
776 reproduced, except for plume #1 with better intensity results. We have already seen in the previous case study
777 that emissions in Asia may be underestimated, especially in the EDGARv4.2 inventory.
778 Similar comparisons were performed in the four case studies selected to estimate and validate the anthropogenic
779 emission inventories coupled with the FLEXPART model. Results are summarized in Table 3. For three of the
780 cases, SOFT-IO simulations showed a better agreement with observations when using MACCity than when
781 using EDGARv4.2. In the fourth case both inventories performed equally well. One reason for the better
782 performance of MACCity is the fact that it provides monthly information (Table 2).

783

784 4.2 Biomass burning emission inventories

785 In order to evaluate and choose biomass burning emission inventories, we have selected eleven case studies with
786 fire-induced plumes (Table 1). Seven of them focused on North-American biomass burning plumes observed in
787 the free troposphere above Europe (flights on 30th of June, 22nd and 23rd of July 2004) and in the upper
788 troposphere/lower stratosphere above the North Atlantic (29th of June 2004) (e.g. Elguindi et al., 2010; Cammas
789 et al., 2009). Two are related to the fires over Western Europe during the 2003 heat wave (Tressol et al. 2008).
790 The two last ones, on the 30th and 31st of July 2008, focused on biomass burning plumes observed in the ITCZ
791 region above Africa as described in a previous study (Sauvage et al., 2007a).

792 The three datasets selected to represent biomass burning emissions are based on different approaches: GFAS
793 v1.2 (Kaiser et al., 2012) and GFED 4 emissions (Giglio et al., 2013) are calculated daily. GFAS v1.2 presents
794 higher spatial resolution. The ICARTT campaign inventory (Turquety et al., 2007) was specifically designed for
795 North-American fires during the summer of 2004 with additional input from local forest services.

796 Figure 7a illustrates the calculated CO contributions for the different fire emission inventories for one of the case
797 studies, on 22nd of July 2004 above Paris. The observations (black line) show high levels of CO in an air mass in
798 the free troposphere between 3 and 6 km, with mixing ratios 140 ppb above the background (blue line) deduced
799 from measurements. This pollution was attributed to long-range transport of biomass burning emission in North
800 America by Elguindi et al. (2010). Outside of the plume, the CO concentration decreases with altitude, from
801 around 150 ppb near the ground, to 100 ppb background in the upper free troposphere. This last value
802 corresponds to the median CO seasonal value deduced from the IAGOS database (Gressent et al., 2014). CO is
803 not considered as an anomaly near the ground as $C_{UT}^R < C_{UT_season}^R(Q3)$.

804 SOFT-IO simulations were performed for this case using MACCity to represent anthropogenic emissions, and
805 GFAS v1.2 (green line), GFED 4 (yellow line), or the ICARTT campaign inventory (red line). Fire vertical
806 injection is realized using the MIXED approach for the three biomass burning inventories, in order to only
807 evaluate the impact of choosing different emission inventories. In the three simulations, contributions show two

808 peaks, one near the ground that is half due to local anthropogenic emissions and half due to contributions from
809 North American biomass burning and thus not considered in this discussion.

810 The second more intense peak, simulated in the free troposphere where the enhanced CO air masses were
811 sampled, is mostly caused by biomass burning emissions (87% of the total calculated CO, Fig. 7b), originating
812 from North-America (99% of the total enhanced CO). When calculated using the ICARTT campaign inventory,
813 the simulated CO enhancement reaches over 150 ppb, which is 10 ppb higher than the observed mixing ratio
814 above the background (+140 ppb), but only for the upper part of the plume.

815 When using global inventories, the simulated contribution peak reaches 70 ppb using GFASv1.2 and 100 ppb
816 using GFED4, which appears to underestimate the measured enhancement (+140 ppb) by up to 50% to 70%
817 respectively. This comparison demonstrates the large uncertainty in simulated CO caused by the emission
818 inventories, both in the case of biomass burning or anthropogenic emissions. For that reason we aim to provide
819 simulations with different global and regional inventories in for the IAGOS data set.

820 As the ICARTT campaign inventory was created using local observations in addition to satellite products, the
821 large difference in the simulated CO compared to the other inventories may in part be due to different
822 quantification of the total area burned (for GFED, GFAS using the FRP as constraint). Turquety et al. (2007)
823 also discussed the importance of peat land burning during that summer. They estimated that they contributed
824 more than a third of total CO emissions (11 Tg of the 30 Tg emitted during summer 2004).

825
826 Figure 8a shows CO mixing ratios as a function of latitude for a flight from Windhoek (Namibia) to Frankfurt
827 (Germany) in July 2008. Observations indicate that the aircraft flew through polluted air masses around the
828 equator (10°S to 10°N), with +100 (+125) ppb of CO on average (at the most) above the 90 ppb background
829 deduced from seasonal IAGOS mixing ratios over this region. Such CO enhancements have been attributed to
830 regional fires injected through ITCZ convection (Sauvage et al., 2007b).

831 The SOFT-IO simulations (colored lines in Fig. 8a) link these air masses mostly to recent biomass burning
832 (responsible for 68% of the total simulated CO, Fig. 8b) in South Africa (Fig. 8c). The calculated CO shows
833 similar features both with GFED4 (yellow line) and GFASv1.2 (green line). The simulation also captures well
834 the intensity variations of the different peaks: maximum values around the equator, lower ones south and north
835 of the equator. The most intense simulated CO enhancement around the equator fits the observed CO
836 enhancement of +125 ppb better when using GFED4 (90 ppb) than when using GFASv1.2 (75 ppb). However
837 the comparison also reveals an underestimation of the CO anomaly's amplitude by around 10 ppb to 25 ppb on
838 average by SOFT-IO. The model is thus only able to reproduce 75% to 90% of the peak concentrations on
839 average. Stroppiana et al. (2010) indeed showed that there are strong uncertainties in the fire emission
840 inventories over Africa (164 to 367 Tg CO per year).

841 **5 Statistical evaluation of the modeled CO enhancements in pollution plumes**

842 In this section, we present a statistical validation of the SOFT-IO calculations based on the entire IAGOS CO
843 data base (2003-2013). The ability of SOFT-IO in simulating CO anomalies is evaluated compared to in situ
844 measurements in terms of:

- 845 • spatial and temporal frequency of the plumes
- 846 • mixing ratio enhancements in the plumes

847 To achieve this, SOFT-IO performances are investigated over different periods of IAGOS measurements
848 depending on the emission inventory used. Three of the four global inventories selected previously (MACCcity,
849 GFAS v1.2, GFED4) are available between 2003 and 2013. EDGAR v4.2 ends in 2008. In the following
850 sections (Sect.5.1 and 5.2), we discuss in detail the results obtained with MACCcity and GFAS v1.2 between
851 2003 and 2013. Other emission inventory combinations are discussed in Sect. 5.3 when investigating SOFT-IO
852 sensitivity to input parameters.

853 **5.1 Detection frequency of the observed plumes with SOFT-IO**

854 The ability of SOFT-IO to reproduce CO enhancements was investigated using CO plumes obtained applying the
855 methodology described in Sect. 3.4 on all flights of the IAGOS database between 2003 and 2013. The frequency
856 of simulated plumes that coincide with the observed C^A anomalies is then calculated. Simulated plumes are
857 considered when matching in time and space the observed plumes, while modeled CO is on average higher than
858 5 ppb within the plume. Note that at this stage, we do not consider the intensity of the plumes.

859 The resulting detection rates are presented in Fig. 9 for eight of the eleven regions shown in Fig. 4. Statistics are
860 presented separately for three altitude levels (Lower Troposphere 0-2 km, Middle Troposphere 2-8 km and
861 Upper Troposphere > 8 km). Figure 9 shows that SOFT-IO performance in detecting plumes is very good and
862 not strongly altitude or region-dependent. In the three layers (LT, MT and UT), detection rates are higher than
863 95% and even close to 100% in the LT where CO anomalies are often related to short-range transport. Detection
864 frequency slightly decreases in the MT and the UT where CO modeling accuracy suffers from larger errors in
865 vertical and horizontal transport. On the contrary CO anomalies in the LT are most of the times related to short-
866 range transport of local pollution, which are well represented in SOFT-IO. For four regions we found worse
867 results: South America MT and UT, Africa MT and North Asia UT but with still high detection frequency (82%
868 to 85%). Note that only relatively few plumes (313 to 3761) were sampled by the IAGOS aircraft fleet in these
869 regions.

870

871 **5.2 Intensity of the simulated plumes**

872 The second objective of SOFT-IO is to accurately simulate the intensity of the observed CO anomalies. Fig. 10a
873 displays the bias between the means of the observed and modeled plumes for the regions sampled by IAGOS and
874 in the three vertical layers (LT, MT and UT), and the bias of the standard deviations in black. As explained
875 above this bias is calculated for the 2003-2013 period and using both anthropogenic emission from MACCcity
876 and biomass burning emissions from GFAS v1.2 and the APT plume detection methodology described in Sect.
877 3.4.

878 The most documented regions presenting CO polluted plumes (Europe, North America, Africa, North Atlantic
879 UT, Central Asia MT and UT, South America, South Asia UT) present low biases (lower than ± 5 ppb, and up to
880 ± 10 ppb for Central Asia MT, South America UT) and low bias of the standard deviations (± 10 ppb to ± 50
881 ppb), which demonstrate a high skill of SOFT-IO.

882 Over several other regions with less frequent IAGOS flights, however, biases are higher, around ± 10 -15 ppb for
883 Africa UT and South Asia MT; around ± 25 -50 ppb for Central Asia LT, South Asia LT and North Asia UT.
884 Except for the last region, the highest biases are found in the Asian lower troposphere, suggesting

885 misrepresentation of local emissions. This is supported by the highest biases of the standard deviations (from \pm
886 60 ppb to \pm 160 ppb for Asian regions). Indeed there is a rapid increase of emissions in this large area (Tanimoto
887 et al., 2009) associated with high discrepancies between different emission inventories (Wang et al., 2013; Stein
888 et al., 2014) and underestimated emissions (Zhang et al., 2015).

889 It is important to note that the biases remain of the same order (\pm 10-15 ppb) when comparing the first (Q1),
890 second (Q2) and third (Q3) quartiles of the CO anomalies observed and modeled within most of the regions (Fig.
891 10b). This confirms the good capacity of the SOFT-IO software in reproducing the CO mixing ratios anomaly in
892 most of the observed pollution plumes.

893 Differences become much larger when considering outlier values of CO anomalies (lower and upper whiskers, \pm
894 2.7σ or 99.3%, Fig. 10b), which means for exceptional events of very low and very high CO enhancements
895 (accounting for 1.4% of the CO plumes), with biases from \pm 10 ppb to \pm 50 ppb for most of the regions. Higher
896 discrepancies are found in the lower and the upper troposphere in two specific regions (North Asia UT and South
897 Asia LT) for these extreme CO anomalies. North Asia UT discrepancies varies from -100 ppb to +200 ppb and
898 from -50 ppb to +100 ppb for South Asia LT. Note that North Asia UT and South Asia LT present respectively
899 extreme pollution events related to pyro-convection (Nédélec et al., 2005) for the first region, and to strong
900 anthropogenic surface emissions (Zhang et al., 2012) for the second one. It may suggest that the model fails to
901 correctly reproduce the transport for some specific but rare events of pyro-convection, or these emission
902 inventories are under estimated for such specific events.

903 When looking at the origin of the different CO anomalies (Fig. 10c), most of them are dominated by
904 anthropogenic emissions, which account for more than 70% of the contributions on average, except for South
905 America and Africa, which are strongly influenced by biomass burning (Sauvage et al. 2005, 2007c; Yamasoe et
906 al., 2014). Discussing origins of the CO anomalies in detail is out of the scope of this study, but gives here some
907 sense on the model performance. It is interesting to note that two of the three regions most influenced by
908 anthropogenic emissions, South Asia LT and Central Asia LT, with more than 90% of the enhanced CO coming
909 from anthropogenic emissions, are the highest biased regions compared to observations. This is not the case for
910 Europe LT for example, which also has a high anthropogenic influence. As stated before, anthropogenic
911 emissions in Asia are more uncertain than elsewhere (Stein et al., 2014).

912

913 In order to go a step further in the evaluation of SOFT-IO in reproducing CO anomalies mixing ratios, Fig. 11
914 displays the monthly mean time series of the observed (black line) and calculated (blue line) CO anomalies in
915 three vertical layers (LT, MT and UT), and the standard deviation of the observations (gray) and calculations
916 (light blue). This graph provides higher temporal resolution of the anomalies. CO polluted plumes are displayed
917 here using MACCity and GFAS v1.2 over the 2003-2013 periods and for the two regions with the largest
918 number of observed CO anomalies, Europe and North America.

919 It is worth noting the good ability of SOFT-IO in quantitatively reproducing the CO enhancements observed by
920 IAGOS. This is especially noticeable in the LT and UT, with similar CO mixing ratios observed and modeled
921 during the entire period and within the standard deviation of the measurements. Standard deviation of the
922 observations is higher in LT where there are fewer measurements than in the UT. However, the amplitude of the
923 seasonal cycle of CO maxima is highly underestimated (-100%) after January 2009 in the European LT, where
924 anthropogenic sources are predominant with more than 90% influence (Fig. 10c). This suggests

925 misrepresentation of anthropogenic emissions in Europe after the year 2009. Indeed Stein et al., (2014)
926 suggested the lower near-surface CO bias was found in Europe in relation with possible under
927 estimation of traffic emissions in the inventories.

928 In the middle troposphere (2-8 km), the CO plumes are systematically overestimated by SOFT-IO by
929 50% to 100% compared to the observations, with larger standard deviation and higher overestimation
930 over NAM. This might be related to different reasons:

- 931 • the chosen methodology of the CO plume enhancements detection for those altitudes
932 (described in Sect. 3.4), which may lead to a large number of plumes with small CO
933 enhancements, which are difficult to simulate. This could be due to the difficulty in defining a
934 realistic CO background in the middle troposphere.
- 935 • the source-receptor transport which may be more difficult to simulate between 2-8 km than in
936 the LT where receptors are close to sources; or than in the UT where most of the plumes are
937 related to convection detrainment better represented in the models than MT detrainment which
938 might be less intense.
- 939 • The frequency of the IAGOS observations which is lower in the LT and in the MT than in the
940 UT.
- 941 • Higher overestimation over NAM MT than Eur MT could be first related to lower frequency
942 of measurements in the NAM. Moreover overestimation is greater during summer when NAM
943 MT is closer to summer sources such as boreal fires, while Eur MT is related to CO air masses
944 more diluted with background air during transatlantic transport.

945 Correlation coefficients between simulated and observed plumes are highest in the LT (0.56 to 0.79) and lower
946 (0.30 to 0.46) in the MT and in the UT, suggesting some difficulties for the model in lifting up pollution from the
947 surface to the UT.

948 **5.3 Sensitivity of SOFT-IO to input parameters**

949 Different factors influence the ability of SOFT-IO to correctly reproduce CO pollution plumes. Among them,
950 transport parameterizations (related to convection, turbulence, etc) are not evaluated in this study as they are
951 inherent of the FLEXPART model. In this section, the model sensitivity to the chosen emission inventory is
952 evaluated. For this, a set of sensitivity studies is performed to investigate different configurations of the emission
953 inventories :

- 954 • type of inventory: MACCity, EDGAR for anthropogenic, GFED4, GFAS v1.2 or ICARTT for biomass
955 burning
- 956 • biomass burning injection heights: DENTENER, MIXED or APT approach (detailed in Sect. 3.3).

957
958 SOFT-IO performances are then investigated using Taylor diagrams (Taylor et al. 2001). The methodology
959 (choice of regions, vertical layers, sampling periods) is similar to the one used to analyze the ability of the model
960 to correctly reproduce the frequency and the intensity of the CO plumes with MACCity and GFAS (Sect.5.1 and
961 Sec5.2).

962 **5.3.1 Anthropogenic emission inventories**

963 Sensitivity of SOFT-IO to anthropogenic emissions is investigated between 2002 and 2008, using GFAS with
964 MACCcity or EDGARv4.2. Fig. 12a presents a Taylor diagram for the two configurations (dots for MACCcity,
965 crosses for EDGAR) for the regions and for the vertical layers described previously (Sect. 5.1 and Sect. 5.2),
966 while Fig. 12b represents the mean bias between each model configuration and the IAGOS observations.

967 As already seen in Sect. 4.1 for the case studies chosen to investigate anthropogenic emissions, slightly better
968 results seem to be obtained with MACCcity. The Taylor diagram shows for most of the regions higher
969 correlations and lower biases in this case. These results are not surprising, as MACCcity (Lamarque et al., 2010;
970 Grenier et al., 2011) is a more recent inventory compared to EDGARv4.2 (Janssens-Maenhout et al., 2010), and
971 expected to better represent anthropogenic emissions. However as stated in Lamarque et al., (2010) both
972 inventories share many aspects (for example over Latin and South America), and the differences between the
973 two inventories are most of the time very low, as global emission inventories tend to be quite similar.

974 Regionally, however, results with EDGARv4.2 can be better by almost 50%, such as over South Asia LT and
975 MT, Central Asia LT and MT. This supports our choice of maintaining several different inventories in SOFT-IO.

976 **5.3.2 Biomass burning emissions**

977 We first investigate the sensitivity of SOFT-IO to the type of biomass burning inventory, using MACCcity with
978 GFAS v1.2 or GFED 4 (2003-2013), using the same MIXED methodology for vertical injection of emissions
979 (Fig. 2). As for anthropogenic emissions, Fig. 13 represents the Taylor diagram and averaged biases for the
980 different configurations.

981 Performances (correlations, standard deviations and biases) are very similar for both biomass burning
982 inventories, with smaller differences compared to anthropogenic inventories. Even for regions dominated by
983 biomass burning such as Africa or South America as depicted previously (Fig. 11c), the sensitivity of the SOFT-
984 IO performance to the type of global fire inventory is below 5 ppb.

985
986 Based on case studies, we discussed in Sect. 4.2 the comparison of CO contributions modeled using regional fire
987 emission inventories. It resulted in a better representation of biomass burning plumes using the specifically
988 designed campaign inventory than using the global inventories (Table 4). However, there is no clear evidence of
989 this result when investigating the model performances during the whole summer 2008. On contrary to Sect. 4.2,
990 it is hard to conclude of systematic better results using the ICARTT inventory. While simulations (not shown)
991 give better results for a few specific events of very high CO using ICARTT, similarly good results are obtained
992 when using GFASv1.2 or GFED4 for most other cases. It is worth noting that IAGOS samples biomass burning
993 plumes far from ICARTT sources, after dispersion and diffusion during transport in the atmosphere. Besides,
994 few boreal fire plumes (that would be better represented using ICARTT), are sampled by the IAGOS program.

995
996 Secondly, we investigate the influence of the vertical injection scheme for the biomass burning emissions, using
997 the three methodologies for determining injection heights described in Sect. 3.3. Sensitivity tests (Fig. 13c and
998 Fig 13d) demonstrate a small influence of the injection scheme on the simulated plumes. The largest influence is
999 found over North Asia UT, where pyro-convection has been highlighted in the IAGOS observations (Nédélec et
1000 al., 2005), with however less than 5 ppb difference between the different schemes. More generally, small vertical

1001 injection influence is probably due to too few cases where boreal fire emissions are injected outside the PBL by
1002 pyro-convection, as shown in the Paugam et al. (2016) study, combined with a too low sampling frequency of
1003 boreal fire plumes by IAGOS.

1004

1005 **6 Conclusions**

1006

1007 Analyzing long term in situ observations of trace gases can be difficult without a priori knowledge of the
1008 processes driving their distribution and seasonal/regional variability, like transport and photochemistry. This is
1009 particularly the case for the extensive IAGOS database, which provides a large number of aircraft-based in-situ
1010 observations (more than 51000 flights so far) distributed on a global scale, and with no a priori sampling
1011 strategy, unlike dedicated field campaigns.

1012

1013 In order to help studying and analyzing such a large data set of in situ observations, we developed a system that
1014 allows quantifying the origin of trace gases both in terms of geographical location as well as source type. The
1015 SOFT-IO module (<https://doi.org/10.25326/2>) is based on the FLEXPART particle dispersion model that is run
1016 backward from each trace gas observation, and on different emission inventories (EDGAR v4.2, MACCity,
1017 GFED 4, GFAS v1.2) than can be easily changed.

1018

1019 The main advantages of the SOFT-IO module are:

1020 • Its flexibility. Source-receptor relationships pre-calculated with the FLEXPART particle dispersion
1021 model can be coupled easily with different emission inventories, allowing each user to select model
1022 results based on a range of different available emission inventories.

1023 • CO calculation, which is computationally very efficient, can be repeated easily whenever updated
1024 emission information becomes available without running again the FLEXPART model. It can also be
1025 extended to a larger number of emission datasets, particularly when new inventories become available,
1026 or for emission inventories inter-comparisons. It can also be extended to other species with similar or
1027 longer lifetime as CO to study other type of pollution sources.

1028 • High sensitivity of the SOFT-IO CO mixing ratios to source choice for very specific regions and case
1029 studies, especially in the LT most of the time driven by local or regional emissions, may also help
1030 improving emission inventories estimates through evaluation with a large database such as IAGOS one.
1031 Indeed as it is based on a Lagrangian dispersion model, the tool presented here is able to reproduce
1032 small-scale variations, which facilitates comparison to in situ observations. It can then be used to
1033 validate emission inventories by confronting them to downwind observations of the atmospheric
1034 composition, using large database of in situ observations of recent pollution.

1035 • More generally SOFT-IO can be used in the future for any kind of atmospheric observations (e.g.
1036 ground based measurements, satellite instruments, aircraft campaigns) of passive tracers.

1037

1038 In this study SOFT-IO is applied to all IAGOS CO observations, using ECMWF operational meteorological
1039 analysis and 3-hour forecast fields and inventories of anthropogenic and biomass burning emissions available on

1040 the ECCAD portal. SOFT-IO outputs are evaluated first at the examples of case studies of anthropogenic and
1041 biomass burning pollution events. The evaluation is then extended statistically, for the entire 2003-2013 period,
1042 over 14 regions and 3 vertical layers of the troposphere.

1043

1044 The main results are the following:

- 1045 • By calculating the contributions of recent emissions to the CO mixing ratio along the flight tracks,
1046 SOFT-IO identifies the source regions responsible for the observed pollution events, and is able to
1047 attribute such plumes to anthropogenic and/or biomass burning emissions.
- 1048 • On average, SOFT-IO detects 95% of all observed CO plumes. In certain regions, detection frequency
1049 reaches almost 100%.
- 1050 • SOFT-IO gives a good estimation of the CO mixing ratio enhancements for the majority of the regions
1051 and the vertical layers. In majority, the CO contribution is reproduced with a mean bias lower than 10-
1052 15 ppb, except for the measurements in the LT of Central and South Asia and in the UT of North Asia
1053 where emission inventories seems to be less accurate.
- 1054 • CO anomalies calculated by SOFT-IO are very close to observations in the LT and UT where most of
1055 the IAGOS data are recorded. Agreement is lower in the MT, possibly because of numerous thinner
1056 plumes of lower intensity (maybe linked to the methodology of the plume selection).
- 1057 • SOFT-IO has less skill in modeling CO in extreme plume enhancements with biases higher than 50 ppb.
1058

1059 In its current version, SOFT-IO is limited by different parameters, such as inherent parameterization of the
1060 Lagrangian model, but also by input of external parameters such as meteorological field analysis and emission
1061 inventories. Sensitivity analyses were then performed using different meteorological analysis and emissions
1062 inventories, and are summarized as follow:

- 1063 • Model results were not very sensitive to the resolution of the meteorological input data. Increasing the
1064 resolution from 1 deg to 0.5 deg resulted only in minor improvements. On the other hand, using
1065 operational meteorological analysis allowed more accurate simulations than using ERA-Interim
1066 reanalysis data, perhaps related to the better vertical resolution of the former.
- 1067 • Concerning anthropogenic emissions sensitivity tests, results display regional differences depending on
1068 the emission inventory choice. Slightly better results are obtained using MACCity.
- 1069 • Model results were not sensitive to biomass burning global inventories, with good results using either
1070 GFED 4 or GFAS v1.2. However, a regional emission inventory shows better results for few individual
1071 cases with high CO enhancements. There is a low sensitivity to parameterizing the altitude of fire
1072 emission injection, probably because events of fires injected outside of the PBL are rare or because
1073 IAGOS does not frequently sample of such events

1074

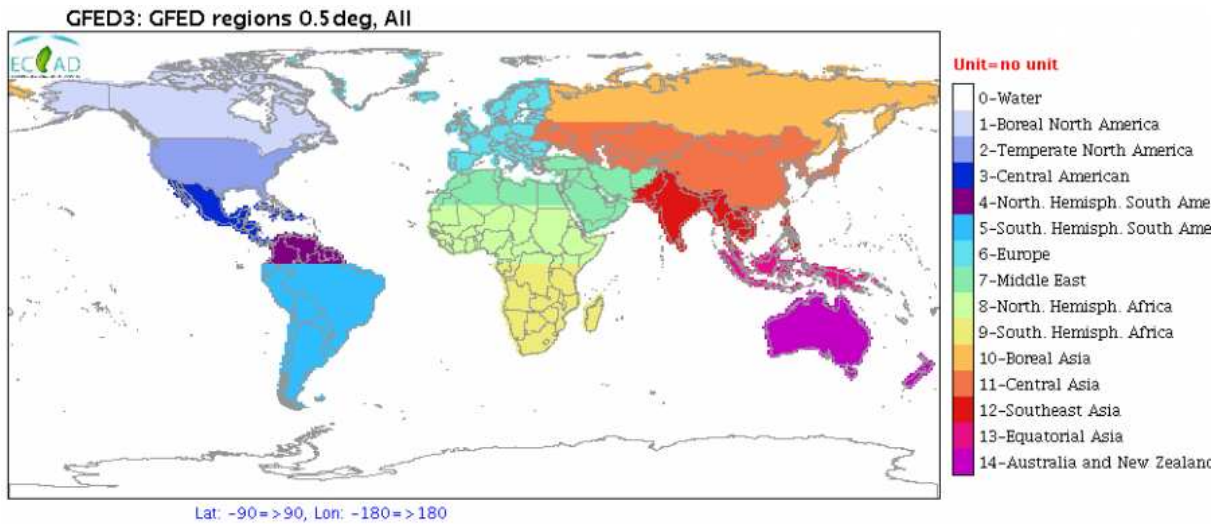
1075 Using such CO calculations and partitioning makes it possible to link the trends in the atmospheric composition
1076 with changes in the transport pathways and/or changes of the emissions.

1077 SOFT-IO products will be made available through the IAGOS central database (<http://iagos.sedoo.fr/#L4Place>)
1078 and are part of the ancillary products (<https://doi.org/10.25326/3>)

1079

1080

1081 **7 Supplements**

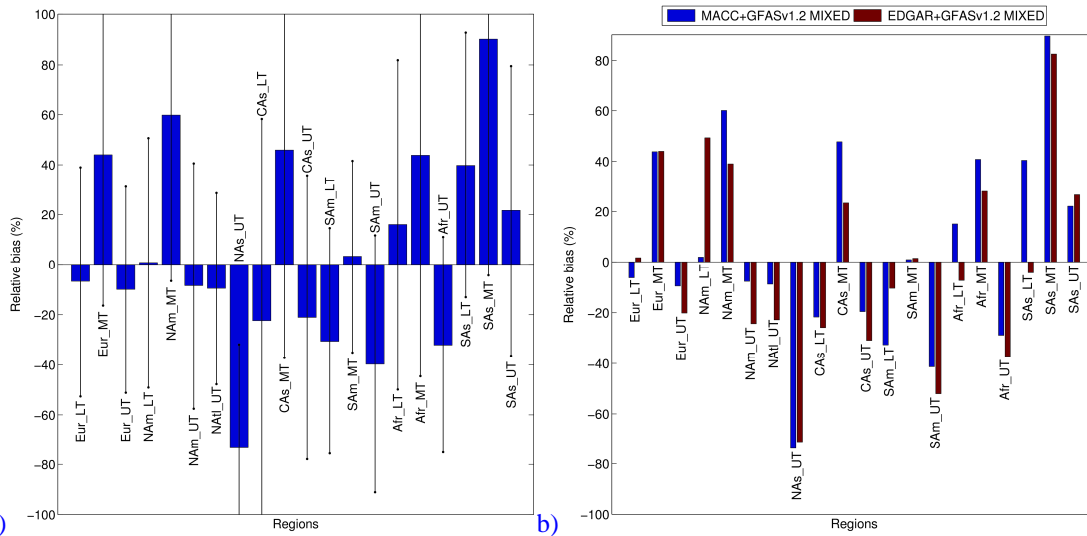


1082

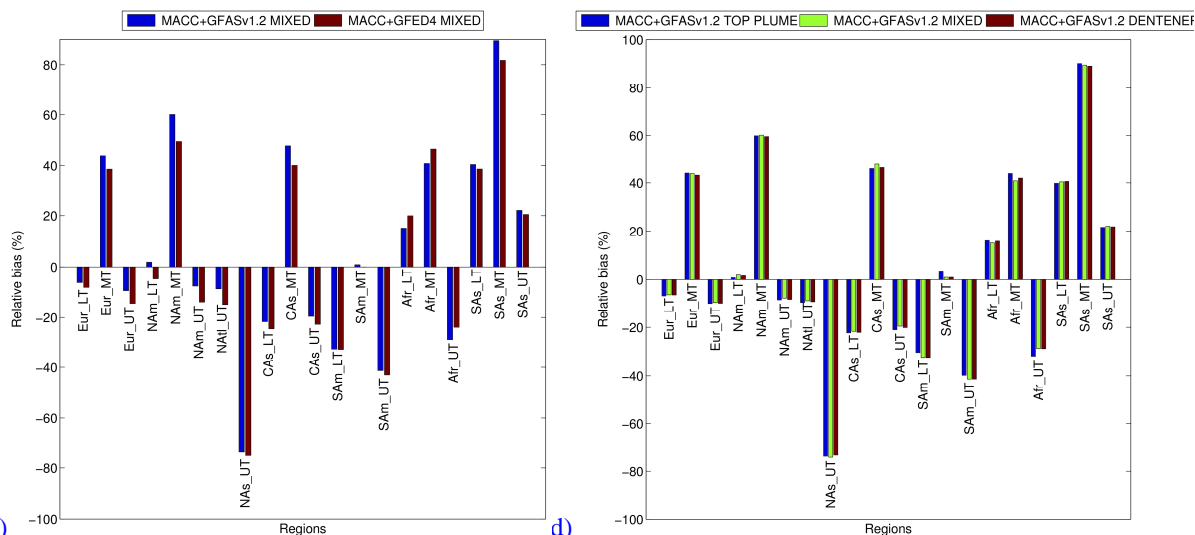
1083

1084 **Figure S1: regions used to discriminate CO origin calculated with SOFT-IO, from**
1085 <http://www.globalfiredata.org/data.html>

1086



1087



1088 c) d)
 1089 **Figure S2: Same as Figs. 10a, 12a, 13b and 13d (a, b, c, d respectively) but for relative bias (%)**

1090 **Acknowledgements**

1091
 1092 The authors would like to thanks ECCAD project for providing emission inventories. The authors acknowledge
 1093 the strong support of the European Commission, Airbus, and the Airlines (Lufthansa, Air-France, Austrian, Air
 1094 Namibia, Cathay Pacific, Iberia and China Airlines so far) who carry the MOZAIC or IAGOS equipment and
 1095 perform the maintenance since 1994. In its last 10 years of operation, MOZAIC has been funded by INSU-
 1096 CNRS (France), Météo-France, Université Paul Sabatier (Toulouse, France) and Research Center Jülich (FZJ,
 1097 Jülich, Germany). IAGOS has been additionally funded by the EU projects IAGOS-DS and IAGOS-ERI. The
 1098 MOZAIC-IAGOS database is supported by AERIS (CNES and INSU-CNRS). The former CNES-ETHER
 1099 program has funded this project.

1100
 1101
 1102

1103 **References**

1104

1105 Barret, B., Sauvage, B., Bennouna, Y., and Le Flochmoen, E.: Upper-tropospheric CO and O₃ budget during the
1106 Asian summer monsoon, *Atmos. Chem. Phys.*, 16, 9129-9147, doi:10.5194/acp-16-9129-2016, 2016

1107 Beirle, S; Spichtinger, N; Stohl, A; et al.: Estimating the NO(x) produced by lightning from GOME and NLDN
1108 data: a case study in the Gulf of Mexico, *Atm. Chem. Phys.*, 6, 1075-1089, 2006.

1109 Boden, T.A., G. Marland, and R.J. Andres. 2015. Global, Regional, and National Fossil-Fuel CO₂ Emissions.
1110 Carbon Dioxide Information Analysis Center, Oak Ridge National Laboratory, U.S. Department of Energy, Oak
1111 Ridge, Tenn., U.S.A. doi 10.3334/CDIAC/00001_V2015, 2015

1112 Cammas, J.-P., Brioude, J., Chaboureau, J.-P., Duron, J., Mari, C., Mascart, P., N'ed'elec, P., Smit, H., Pätz,
1113 H.W., Volz-Thomas, A., Stohl, A., and Fromm, M.: Injection in the lower stratosphere of biomass fire emissions
1114 followed by long-range transport: a MOZAIC case study, *Atm. Chem. Phys.*, 9, 5829-5846, [http://www. atmos-
1115 chem-phys.net/9/5829/2009/](http://www.atmos-chem-phys.net/9/5829/2009/), 2009.

1116 Clark, Hannah, Bastien Sauvage, Valerie Thouret, Philippe Nedelec, Romain Blot, Kuo-Ying Wang, Herman
1117 Smit, et al.: The First Regular Measurements of Ozone, Carbon Monoxide and Water Vapour in the Pacific
1118 UTLS by IAGOS, *Tellus B*, 67. doi:10.3402/tellusb.v67.28385, 2015.

1119 Cooper, O. R.; Stohl, A.; Trainer, M.; et al : Large upper tropospheric ozone enhancements above midlatitude
1120 North America during summer: In situ evidence from the IONS and MOZAIC ozone measurement network, *J.*
1121 *Geophys. Res.*, 111, D24, 2006.

1122 Cristofanelli, P., Fierli, F., Marinoni, A., Calzolari, F., Duchi, R., Burkhart, J., Stohl, A., Maione, M., Arduini, J.,
1123 and Bonasoni, P.: Influence of biomass burning and anthropogenic emissions on ozone, carbon monoxide and
1124 black carbon at the Mt. Cimone GAW-WMO global station (Italy, 2165 m a.s.l.), *Atmos. Chem. Phys.*, 13, 15-
1125 30, doi:10.5194/acp-13-15-2013, 2013

1126 Damoah, R., Spichtinger, N., Forster, C., James, P., Mattis, I., Wandinger, U., Beirle, S., Wagner, T., and Stohl,
1127 A.: Around the world in 17 days -hemispheric-scale transport of forest fire smoke from Russia in May 2003,
1128 *Atm. Chem. Phys.*, 4, 1311-1321, 2004.

1129 Dentener, F., Kinne, S., Bond, T., Boucher, O., Cofala, J., Generoso, S., Ginoux, P., Gong, S., Hoelzemann, J. J.,
1130 Ito, A., Marelli, L., Penner, J. E., Putaud, J.-P., Textor, C., Schulz, M., van der Werf, G. R., and Wilson, J.:
1131 Emissions of primary aerosol and precursor gases in the years 2000 and 1750 prescribed data-sets for AeroCom,
1132 *Atmos. Chem. Phys.*, 6, 4321-4344, doi:10.5194/acp-6-4321-2006, 2006

1133 Ding, A., T. Wang, and C. Fu (2013), Transport characteristics and origins of carbon monoxide and ozone in
1134 Hong Kong, South China, *J. Geophys. Res. Atmos.*, 118, 9475-9488, doi:10.1002/jgrd.50714, 2013

1135 Eastham, S. D. and Jacob, D. J.: Limits on the ability of global Eulerian models to resolve intercontinental
1136 transport of chemical plumes, *Atmos. Chem. Phys.*, 17, 2543-2553, doi:10.5194/acp-17-2543-2017, 2017.

1137 Elguindi, N., Clark, H., Ordonez, C., Thouret, V., Flemming, J., Stein, O., Huijnen, V., Moinat, P., Inness, A.,
1138 Peuch, V.-H., Stohl, A., Turquety, S., Athier, G., Cammas, J.-P., and Schultz, M.: Current status of the ability of
1139 the GEMS/MACC models to reproduce the tropospheric CO vertical distribution as measured by MOZAIC,
1140 *Geosci. Model Dev.*, 3, 501-518, <http://www.geosci-model-dev.net/3/501/2010/>, 2010.

1141 Freitas, S. R., Longo, K. M., Chatfield, R., Latham, D., Silva Dias, M. A. F., Andreae, M. O., Prins, E., Santos, J.
1142 C., Gielow, R., and Carvalho Jr., J. A.: Including the sub-grid scale plume rise of vegetation fires in low

1143 resolution atmospheric transport models, *Atmos. Chem. Phys.*, 7, 3385-3398, doi:10.5194/acp-7-3385-2007,
1144 2007

1145 Giglio, S., Randerson, J.T., Van der Werf, G.R.: Analysis of daily, monthly, and annual burned area using the
1146 fourth-generation global fire emissions database (GFED4), *J. Geophys. Res.*, 10.1002/jgrg.20042, 2013

1147 Good, P., Giannakopoulos, C., O'Connor, F.M., Arnold, S.R., de Reus, M., Schlager, H.: Constraining
1148 tropospheric mixing timescales using airborne observations and numerical models, *Atm. Chem. Phys.*, 3, 1023-
1149 1035, 2003.

1150 Granier, C., Bessagnet, B., Bond, T., D'Angiola, A., Denier van der Gon, H., Frost, G., Heil, A., Kaiser, J.,
1151 Kinne, S., Klimont, Z., Kloster, S., Lamarque, J.-F., Liousse, C., Masui, T., Meleux, F., Mieville, A., Ohara, T.,
1152 Raut, J.-C., Riahi, K., Schultz, M., Smith, S., Thompson, A., van Aardenne, J., van der Werf, G., and van
1153 Vuuren, D.: Evolution of anthropogenic and biomass burning emissions of air pollutants at global and regional
1154 scales during the 1980-2010 period, *Climatic Change*, 109, 163–190, [http://dx.doi.org/10.1007/s10584-011-](http://dx.doi.org/10.1007/s10584-011-0154-1)
1155 [0154-1](http://dx.doi.org/10.1007/s10584-011-0154-1), 10.1007/s10584-011-0154-1, 2011.

1156 Granier, C., Damas, S., Liousse, C., Middleton, P., Mieville, A., et al. : The ECCAD Database: Emissions of
1157 Atmospheric Compounds & Compilation of Ancillary Data. IGAC Newsletter, pp.18-20, 2012

1158 Gressent, A., Sauvage, B., Defer, E. et al. : Lightning NO_x influence on large-scale NO_y and O₃ plumes
1159 observed over the northern mid-latitudes, *Tellus B*, 66, 25544, 2014

1160 Hanna, S. R.: Applications in air pollution modeling, *Atmospheric Turbulence and Air Pollution Modelling*,
1161 1982.

1162 Jacob, D.J.: Introduction to Atmospheric Chemistry, Princeton University Press, 1999

1163 Janssens-Maenhout, G., Petrescu, A. M. R., Muntean, M., and Blujdea, V.: Verifying Greenhouse Gas
1164 Emissions: Methods to Support International Climate Agreements, *Greenhouse Gas Measurement and*
1165 *Management*, 2010.

1166 Kaiser, J. W., Heil, A., Andreae, M. O., Benedetti, A., Chubarova, N., Jones, L., Morcrette, J. J., Razinger, M.,
1167 Schultz, M. G., Suttie, M., and van der Werf, G. R.: Biomass burning emissions estimated with a global fire
1168 assimilation system based on observed fire radiative power, *Biogeosciences*, 9, 527–554, 2012.

1169 Liu, L., Logan, J.A., Murray, L.T., Pumphrey, H.C., Schwartz, M.J., Megretskaja, I.A.: Transport analysis and
1170 source attribution of seasonal and interannual variability of CO in the tropical upper troposphere and lower
1171 troposphere, *Atm. Chem. Phys.*, 13, 129-146, 2013.

1172 Logan, J.A., Prather, M.J., Wofsy, S.C. et al. : Tropospheric Chemistry – A Global Perspective, *J. Geophys.*
1173 *Res.*, 86, 7210-7254, 1981.

1174 Marengo, A; Thouret, V; Nedelec, P; et al.: Measurement of ozone and water vapor by Airbus in-service aircraft:
1175 The MOZAIC airborne program, An overview, *J. Geophys. Res.*, 103, D19, 1998.

1176 Mauzerall, DL; Logan, JA; Jacob, DJ; et al. : Photochemistry in biomass burning plumes and implications for
1177 tropospheric ozone over the tropical South Atlantic, *J. Geophys. Res.*, 103, D7, 1998.

1178 Miyazaki, K., Eskes, H., Sudo, K., Boersma, K. F., Bowman, K., and Kanaya, Y.: Decadal changes in global
1179 surface NO_x emissions from multi-constituent satellite data assimilation, *Atmos. Chem. Phys.*, 17, 807-837,
1180 doi:10.5194/acp-17-807-2017, 2017

1181 Nédélec, P., Thouret, V., Brioude, J., Sauvage, B., Cammas, J. P., and Stohl, A.: Extreme CO concentrations in
1182 the upper troposphere over northeast Asia in June 2003 from the in situ MOZAIC aircraft data, *Geophys. Res.*
1183 *Lett.*, 32, 2005.

1184 Nedelec, P; Cammas, JP; Thouret, V; et al: An improved infrared carbon monoxide analyser for routine
1185 measurements aboard commercial Airbus aircraft: technical validation and first scientific results of the MOZAIC
1186 III programme, *Atm. Chem. Phys.*, 3, 1551-1564, 2003

1187 Nedelec, P., Blot, R., Boulanger, D. et al.: Instrumentation on commercial aircraft for monitoring the
1188 atmospheric composition on a global scale: the IAGOS system, technical overview of ozone and carbon
1189 monoxide measurements, *Tellus B*, 67, 27791, 2015.

1190 Newell, R.E., Thouret, V., Cho, J.Y.N., Stoller, P., Marenco, A., and Smit, H.G.S.: Ubiquity of quasi-horizontal
1191 layers in the atmosphere, *Nature*, 398, 316-319, doi:10.1038/18642, 1999

1192 Paugam, R., Wooster, M., Atherton, J., Freitas, S. R., Schultz, M. G., and Kaiser, J. W.: Development and
1193 optimization of a wildfire plume rise model based on remote sensing data inputs – Part 2, *Atmos. Chem. Phys.*
1194 *Discuss.*, 15, 9815-9895, doi:10.5194/acpd-15-9815-2015, 2015

1195 Paugam, R., Wooster, M., Freitas, S. R., and Val Martin, M.: A review of approaches to estimate wildfire plume
1196 injection height within large scale atmospheric chemical transport models, *Atmos. Chem. Phys.*, 16, 907-925,
1197 doi:10.5194/acpd-16-907-2016, 2016

1198 Petzold, A., Thouret, V., Gerbig, C. et al.: Global-scale atmosphere monitoring by in-service aircraft –current
1199 achievements and future prospects of the European Research infrastructure IAGOS, *Tellus B*, 67, 28452, 2015

1200 Pisso, I., Real, E., Law, K.S., Legras, B., Bousserez, N., Attié, J.L., Schlager, H.: Estimation of mixing in the
1201 troposphere from Lagrangian trace gas reconstructions during long-range pollution plume transport , *J. of*
1202 *Geophys. Res.* , 114, D19301, 2010.

1203 Rémy, S., Veira, A., Paugam, R., Sofiev, M., Kaiser, J. W., Marenco, F., Burton, S. P., Benedetti, A., Engelen,
1204 R. J., Ferrare, R., and Hair, J. W.: Two global climatologies of daily fire emission injection heights since 2003,
1205 *Atmos. Chem. Phys. Discuss.*, doi:10.5194/acp-2015-1048, in review, 2016

1206 Rodean, H. C.: *Stochastic Lagrangian Models of Turbulent Diffusion*, vol. 26, American Meteorological Society,
1207 1996.

1208 Sauvage, B., Thouret, V., Cammas, J.P., Gheusi, F., Athier, G., and Nédélec P.: Tropospheric ozone over
1209 Equatorial Africa: regional aspects from the MOZAIC data, *Atmos. Chem. Phys.*, 5, 311-335, 2005

1210 Sauvage, B., V. Thouret, A. M. Thompson, J. C. Witte, J.-P. Cammas, P. Nédélec, and G. Athier: Enhanced
1211 view of the “tropical Atlantic ozone paradox” and “zonal wave one” from the in situ MOZAIC and SHADOZ
1212 data, *J. Geophys. Res.*, 111, *D01301*, doi:[10.1029/2005JD006241](https://doi.org/10.1029/2005JD006241), 2006.

1213 Sauvage, B.; Thouret, V.; Cammas, J. -P.; et al.: Meridional ozone gradients in the African upper troposphere,
1214 *Geophys. Res. Lett.*, 34, L03817, 2007a

1215 Sauvage, B., R. V. Martin, A. van Donkelaar, and J. R. Ziemke: Quantification of the factors controlling tropical
1216 tropospheric ozone and the South Atlantic maximum, *J. Geophys. Res.*, 112, D11309,
1217 doi:10.1029/2006JD008008, 2007b

1218 Sauvage B., Martin R.V., van Donkelaar A., Liu X., Chance K., Jaeglé L., Palmer P.I., Wu S. , Fu T.-M. :
1219 Remote sensed and in situ constraints on processes affecting tropical ozone, *Atmospheric Chemistry and*
1220 *Physics*, 7, 815-838, 2007c.

1221 Seibert, P. and Frank, A.: Source-receptor matrix calculation with a Lagrangian particle dispersion model in
1222 backward mode, *Atm. Chem. Phys.*, 4, 51–63, 2004

1223 Staudt, A. C., Jacob, D. J., Logan, J. A., Bachiochi, D., Krishnamurti, T. N., and Sachse, G. W.: Continental
1224 sources, transoceanic transport, and interhemispheric exchange of carbon monoxide over the Pacific, *J. Geophys.*
1225 *Res.*, 106(D23), 32571–32590, 2001

1226 Stein, O., Schultz, M.G., Bouarar, I., Clark, H., Huijnen, V., Gaudel, A., George, M., Clerbaux, C.: On the
1227 wintertime low bias of Northern Hemisphere carbon monoxide found in global model simulations, *Atmos.*
1228 *Chem. Phys.*, 14, 9295-9316, doi:10.5194/acp-14-9295-2014, 2014

1229 Stohl, A., M. Hittenberger, and G. Wotawa: Validation of the Lagrangian particle dispersion model FLEXPART
1230 against large scale tracer experiments, *Atmos. Environ.*, 32, 4245-4264, 1998

1231 Stohl, A. and Thomson, D. J.: A density correction for Lagrangian particle dispersion models, *Boundary Layer*
1232 *Meteorol.*, 90, 155–167, 1999.

1233 Stohl, A., Eckhardt, S., Forster, C., James, P., and Spichtinger, N.: On the pathways and timescales of
1234 intercontinental air pollution transport, *J. Geophys. Res.*, 107, 2002.

1235 Stohl, A., Forster, C., Eckhardt, S., Spichtinger, N., Huntrieser, H., Heland, J., Schlager, H., Wilhelm, S.,
1236 Arnold, F., and Cooper, O.: A backward modeling study of intercontinental pollution transport using aircraft
1237 measurements, *J. Geophys. Res.*, 108, 2003.

1238 Stohl, A., Forster, C., Frank, A., Seibert, P., and Wotawa, G.: Technical note: The Lagrangian particle dispersion
1239 model FLEXPART version 6.2, *Atmos. Chem. Phys.*, 5, 2461-2474, doi:10.5194/acp-5-2461-2005, 2005

1240 Stohl, A., Aamaas, B., Amann, M., Baker, L. H., Bellouin, N., Berntsen, T. K., Boucher, O., Cherian, R.,
1241 Collins, W., Daskalakis, N., Dusinska, M., Eckhardt, S., Fuglestedt, J. S., Harju, M., Heyes, C., Hodnebrog, Ø.,
1242 Hao, J., Im, U., Kanakidou, M., Klimont, Z., Kupiainen, K., Law, K. S., Lund, M. T., Maas, R., MacIntosh, C.
1243 R., Myhre, G., Myriokefalitakis, S., Olivie, D., Quaas, J., Quennehen, B., Raut, J.-C., Rumbold, S. T., Samset, B.
1244 H., Schulz, M., Seland, Ø., Shine, K. P., Skeie, R. B., Wang, S., Yttri, K. E., and Zhu, T.: Evaluating the climate
1245 and air quality impacts of short-lived pollutants, *Atmos. Chem. Phys.*, 15, 10529-10566, doi:10.5194/acp-15-
1246 10529-2015, 2015

1247 Stroppiana, D., Brivio, P. A., Grégoire, J.-M., Liousse, C., Guillaume, B., Granier, C., Mieville, A., Chin, M.,
1248 and Pétron, G.: Comparison of global inventories of CO emissions from biomass burning derived from remotely
1249 sensed data, *Atm. Chem. Phys.*, 10, 12173–12189, <http://www.atmos-chem-phys.net/10/12173/2010/>, 2010.

1250 Tanimoto, H., Ohara, T., Uno, I.: Asian anthropogenic emissions and decadal trends in springtime tropospheric
1251 ozone over Japan: 1998-2007, *Geophys. Res. Letters*, doi: 10.1029/2009GL041382, 2009

1252 Taylor, K. E., Summarizing multiple aspects of model performance in a single diagram, *Journal of Geophysical*
1253 *Research*, 106, D7, 7183-7192, 2001

1254 Tressol, M., Ordonez, C., Zbinden, R., Brioude, J., Thouret, V., Mari, C., Nedelec, P., Cammas, J.-P., Smit, H.,
1255 Patz, H.-W., and Volz-Thomas, A.: Air pollution during the 2003 European heat wave as seen by MOZAIC
1256 airliners, *Atm. Chem. Phys.*, 8, 2133–2150, 2008.

1257 Turquety, S., Logan, J. A., Jacob, D. J., Hudman, R. C., Leung, F. Y., Heald, C. L., Yantosca, R. M., Wu, S.,
1258 Emmons, L. K., Edwards, D. P., and Sachse, G. W.: Inventory of boreal fire emissions for North America in
1259 2004: Importance of peat burning and pyroconvective injection, *J. Geophys. Res.*, 112, 2007.

1260 Van der Werf, G. R., Randerson, J. T., Giglio, L., Collatz, G. J., Mu, M., Kasibhatla, P. S., Morton, D. C.,
1261 DeFries, R. S., Jin, Y., and van Leeuwen, T. T.: Global fire emissions and the contribution of deforestation,
1262 savanna, forest, agricultural, and peat fires (1997-2009), *Atm. Chem. Phys.*, 10, 11 707–11 735, 2010.

1263 Tanimoto, H., Ohara, T., Uno, I.: Asian anthropogenic emissions and decadal trends in springtime tropospheric
1264 ozone over Japan: 1998-2007, *Geophys. Res. Letters*, 36, L23802, doi:10.1029/2009GL041382, 2009

1265 Thouret, V., Cho, J.Y.N., Newell, R.E., Larenco, A. and Smit, H.G.J.: General characteristics of tropospheric
1266 trace constituent layers observed in the MOZAIC program, *J. of Geophys. Res.*, 105, D13, 17379-17392, doi:
1267 10.1029/2000JD900238, 2000

1268 Thouret, V., Cammas, J.-P., Sauvage, B., Athier, G., Zbinden, R., Nédélec, P., Simon, P., and Karcher, F.:
1269 Tropopause referenced ozone climatology and inter-annual variability (1994–2003) from the MOZAIC
1270 programme, *Atmos. Chem. Phys.*, 6, 1033-1051, doi:10.5194/acp-6-1033-2006, 2006

1271 Vay, S. A., , Y. Choi, K. P. Vadrevu, D. R. Blake, S. C. Tyler, A. Wisthaler, A. Hecobian, Y. Kondo, G. S.
1272 Diskin, G. W. Sachse, J-H. Woo, A. J. Weinheimer, J. F. Burkhart, A. Stohl, and P. O. Wennberg : Patterns of
1273 CO₂ and radiocarbon across high northern latitudes during International Polar Year 2008. *J. Geophys. Res.* 116,
1274 D14301, doi:10.1029/2011JD015643, 2011

1275 Wang, X., Wang, Y., Hao, J., Kondo, Y., Irwin, M., Munger, J.W., Zhao, Y.: Top-down estimate of China's
1276 black carbon emissions using surface observations: sensitivity to observation representativeness and transport
1277 model error, *J. of Geophys. Res.*, 118, 5781-5795, doi: 10.1002/jgrd.50397, 2013.

1278 Wen, D., Lin, J.C., Millet, D.B., et al.: A backward-time stochastic Lagrangian air quality model, *Atmos. Env.*
1279 54, 373-386, 2012

1280 Yamasoe, M.A.; Sauvage, B.; Thouret, V.; et al. : Analysis of tropospheric ozone and carbon monoxide profiles
1281 over South America based on MOZAIC/IAGOS database and model simulations, *Tellus B*, 67, 27884, 2015

1282 Yashiro, H., Sugawara, S., Sudo, K., Aoki, S., and Nakazawa, T.: Temporal and spatial variations of carbon
1283 monoxide over the western part of the Pacific Ocean, *J. Geophys. Res.*, 114, D08305, doi:10.1029/2008jd010876,
1284 2009

1285 Zhang, Yiqiang; Liu, Hongyu; Crawford, James H.; et al. : Distribution, variability and sources of tropospheric
1286 ozone over south China in spring: Intensive ozonesonde measurements at five locations and modeling analysis, *J.*
1287 *of Geophys. Res.*, 117, D12304, 2012

1288 Zhang, L., Henze, D.K., Grell, G.A. et al.: Constraining black carbon aerosol over Asia using OMI aerosol
1289 absorption optical depth and the adjoint of GEOS-Chem, *Atmos. Chem. Phys.*, 15, 10281-10308,
1290 doi:10.5194/acp-15-10281-2015, 2015

1291
1292
1293
1294
1295
1296
1297
1298
1299

1300
1301
1302

Date	Take-off	Landing	Used for choosing
10 March 2002	Frankfurt	Denver	Anthropogenic emission inventories
27 November 2002	Dallas	Frankfurt	Anthropogenic emission inventories
4 June 2003	Tokyo	Vienna	Fire injection heights (pyro-convection)
6 August 2003	Boston	Frankfurt	Fire injection heights
9 August 2003	Dubai	Frankfurt	Fire injection heights
10 August 2003	Frankfurt	Dallas	Fire injection heights
29 June 2004	Caracas	Frankfurt	Fire injection heights (pyro-convection)
30 June 2004	Frankfurt	Washington	Fire injection heights (pyro-convection) Fire inventories
22 July 2004	Frankfurt	Atlanta	Fire injection heights (pyro-convection) Fire inventories
22 July 2004	Douala	Paris	Fire injection heights (pyro-convection) Fire inventories
23 July 2004	Frankfurt	Atlanta	Fire injection heights (pyro-convection) Fire inventories
19 July 2005	München	Hong Kong	Anthropogenic emission inventories
22 October 2005	München	Hong Kong	Anthropogenic emission inventories
30 July 2008	Windhoek	Frankfurt	Fire injection heights Fire emission inventories
31 July 2008	Frankfurt	Windhoek	Fire injection heights Fire emission inventories

1303 **Table 1: Case studies used to define model settings. Cases studies discussed in the manuscript are in bold**

1304
1305
1306
1307
1308
1309
1310
1311
1312
1313
1314
1315
1316
1317
1318

Inventory	Temporal coverage	Horizontal resolution	Temporal resolution	Reference
<i>Anthropogenic emissions</i>				
MACCity	1960 – 2014 +	0.5° x 0.5°	Monthly	<i>Lamarque et al., 2010; Granier et al. (2011)</i>
EDGAR v4.2	1970 - 2008	0.5° x 0.5°	Yearly	<i>Janssens-Maenhout et al. (2010)</i>
<i>Biomass Burning emissions</i>				
GFED 4	1997 – 2017+	0.5° x 0.5°	Daily	<i>Giglio et al. (2013)</i>
GFAS v1.0	2002	0.5° x 0.5°	Daily	
GFAS v1.2	2003 – 2017 +	0.1° x 0.1°	Daily	<i>Kaiser et al. (2012)</i>
ICARTT	2004	1° x 1°	Daily	<i>Turquety et al. (2007)</i>

1319 **Table 2: List of emission inventories used in this study.**

1320
1321
1322
1323
1324
1325
1326
1327
1328
1329
1330
1331
1332
1333
1334
1335
1336
1337
1338
1339
1340
1341
1342
1343
1344
1345
1346
1347
1348
1349
1350
1351
1352
1353
1354
1355

Flight	IAGOS anomaly	IAGOS std	MACCity anomaly	MACCity std	EDGAR anomaly	EDGAR std	Anomaly altitude
10 March 2002 Frankfurt – Denver	16.8	8.7	20.2	6.9	12.8	5.1	UT
27 November 2002 Dallas – Frankfurt	28.0	8.6	20.0	8.0	16.4	7.4	UT
19 July 2005 München - Hong Kong	130.1	97.8	45.8	9.7	34.6	7.7	PBL
22 October 2005 München - Hong Kong	157.9	105.1	170.7	109.8	103.9	62.0	PBL

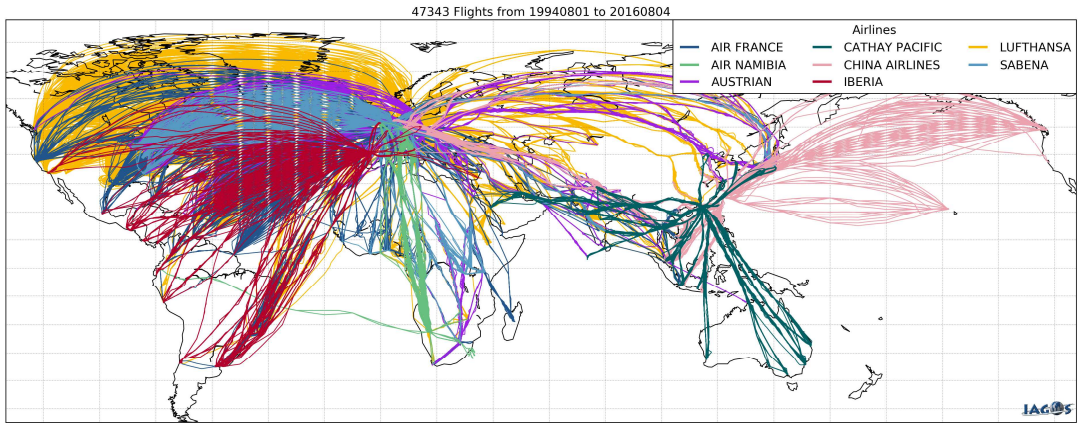
1356 **Table 3. Summary of the averaged observed and simulated anomaly and corresponding averaged standard deviation**
1357 **(std) (in ppb) determined for representing anthropogenic emissions for different case studies (using GFAS v1.2 for**
1358 **biomass burning emissions). Altitude of the anomaly is indicated: boundary layer (PBL); middle troposphere (MT);**
1359 **upper troposphere (UT)**

1360
1361
1362
1363
1364
1365
1366
1367
1368
1369
1370
1371
1372
1373
1374
1375
1376
1377
1378
1379
1380
1381
1382
1383
1384
1385
1386

Flight	IAGOS anomaly	IAGOS std	GFAS v1.2 anomaly	GFAS v1.2 std	GFED4 anomaly	GFED4 std	ICARTT anomaly	ICARTT std	Anomaly altitude
29 June 2004 Caracas - Frankfurt	32.6	33.2	44.4	2.4	43.0	2.3	43.6	2.4	PBL
30 June 2004 Frankfurt - Washington	52.5	34.0	36.6	9.1	25.4	6.6	23.5	5.9	MT
22 July 2004 Frankfurt - Atlanta	87.0	35.0	42.8	17.6	45.8	18.9	39.7	15.7	MT
22 July 2004 Douala - Paris	117.1	24.2	43.5	20.0	55.0	27.2	72.4	42.3	MT
23 July 2004 Frankfurt - Atlanta	78.9	45.4	34.7	22.4	45.3	32.8	46.0	35.9	MT
30 July 2008 Windhoek - Frankfurt	72.9	41.9	33.0	19.2	42.8	26.0	N/A	N/A	UT
31 July 2008 Frankfurt - Windhoek	38.3	32.0	28.1	10.8	34.0	12.8	N/A	N/A	UT

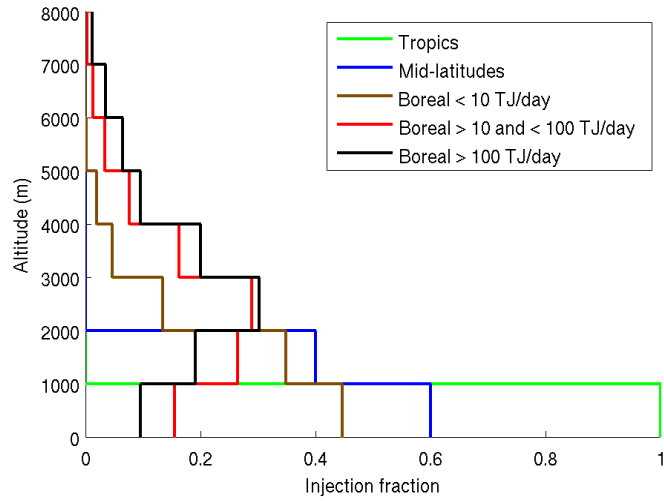
1387 **Table 4. Summary of the averaged observed and simulated anomaly and corresponding averaged standard deviation**
1388 **(std) (in ppb) determined for representing biomass burning emissions for different case studies (using MACCity for**
1389 **anthropogenic emissions). Altitude of the anomaly is indicated: boundary layer (PBL); middle troposphere (MT);**
1390 **upper troposphere (UT). Note that the ICARTT inventory is only available for summer 2004.**

1391
1392
1393
1394
1395
1396
1397
1398
1399
1400
1401
1402
1403
1404
1405
1406
1407



1408
1409 **Figure 1 : Map showing all flights performed by the IAGOS program**

- 1410
- 1411
- 1412
- 1413
- 1414
- 1415
- 1416
- 1417
- 1418
- 1419
- 1420
- 1421
- 1422
- 1423
- 1424
- 1425
- 1426
- 1427
- 1428
- 1429
- 1430
- 1431
- 1432
- 1433



1434 **Figure 2: Injection profiles used for biomass burning emissions for different regions (Tropics, Mid-latitudes, Boreal)**
 1435 **in the MIXED methodology.**
 1436

1437

1438

1439

1440

1441

1442

1443

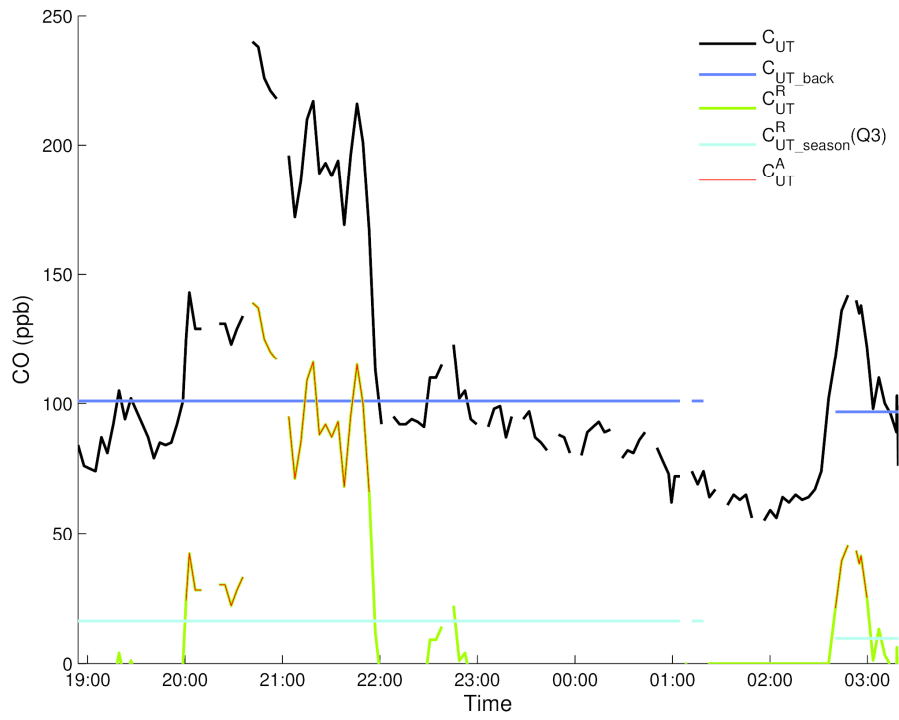
1444

1445

1446

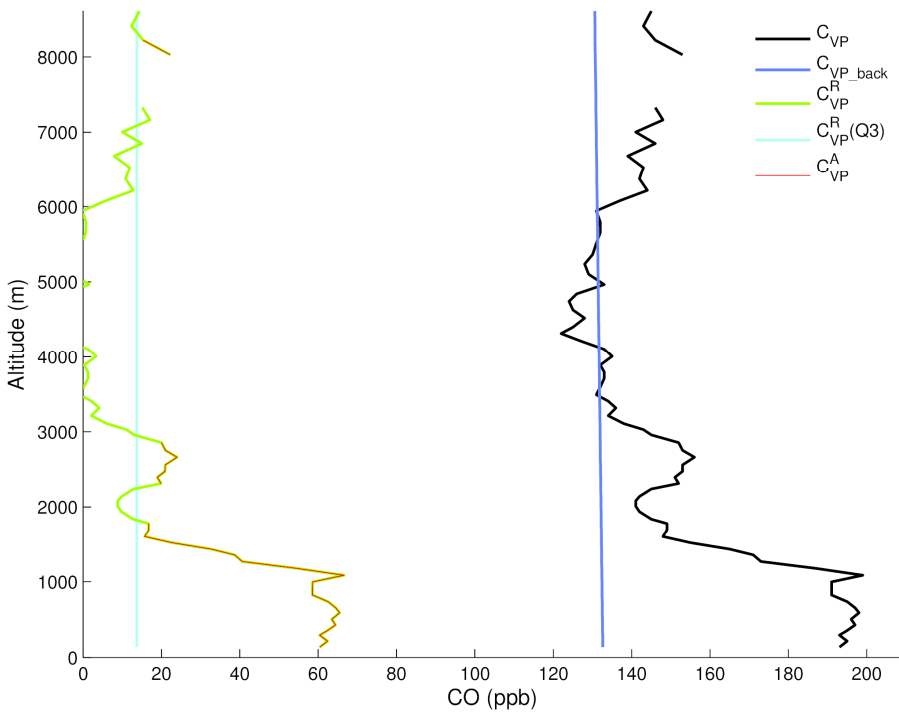
1447

1448



1449

a)



1450

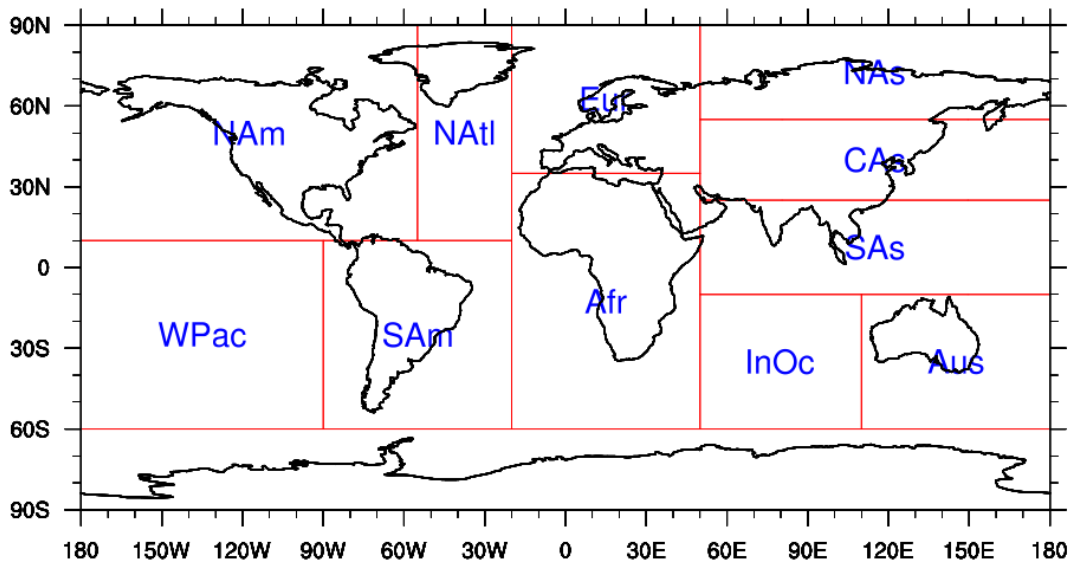
b)

Figure 3: Methodology used to extract CO anomalies along the flight track for (a) the cruise part of the flight and (b) during take off and landing. Further details are given in section 3.4.

1451

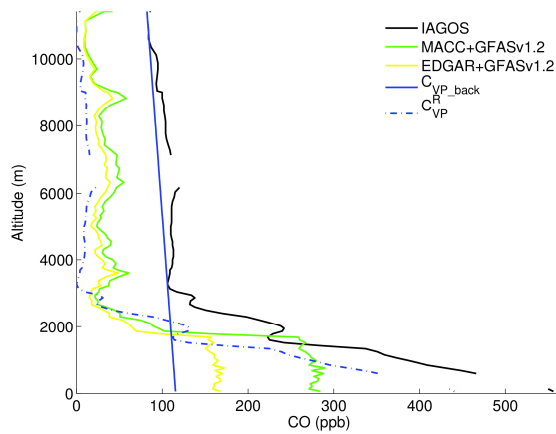
1452

1453

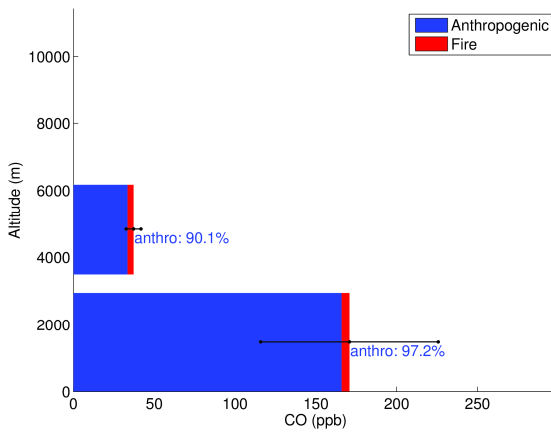


1454
 1455
 1456
 1457
 1458
 1459
 1460
 1461
 1462
 1463
 1464

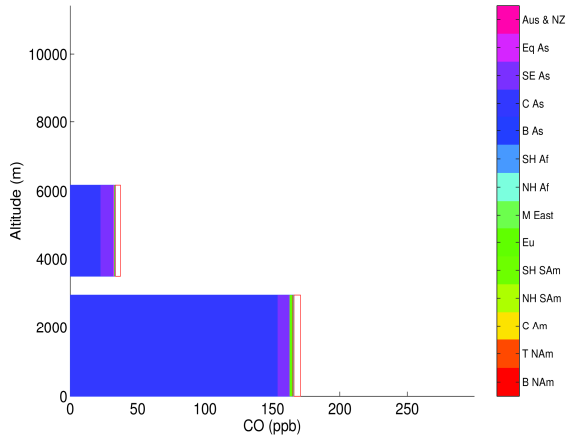
Figure 4: Map of the defined regions used to sort IAGOS CO anomalies



1465 a)



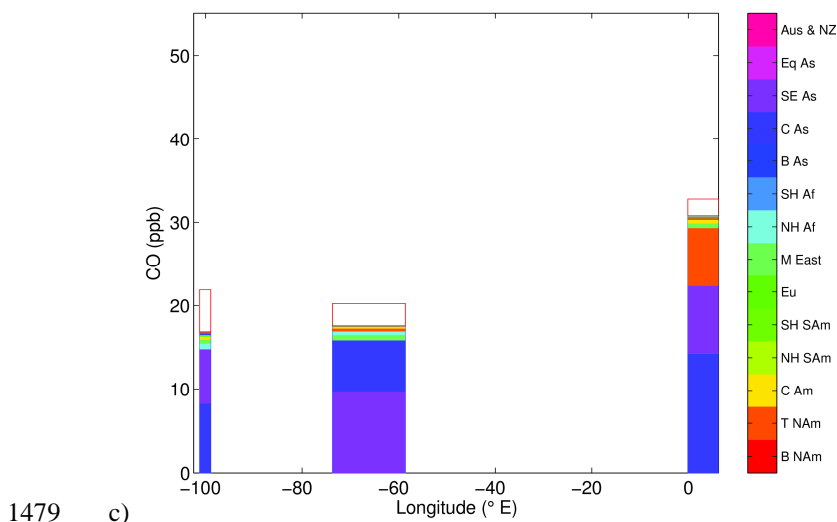
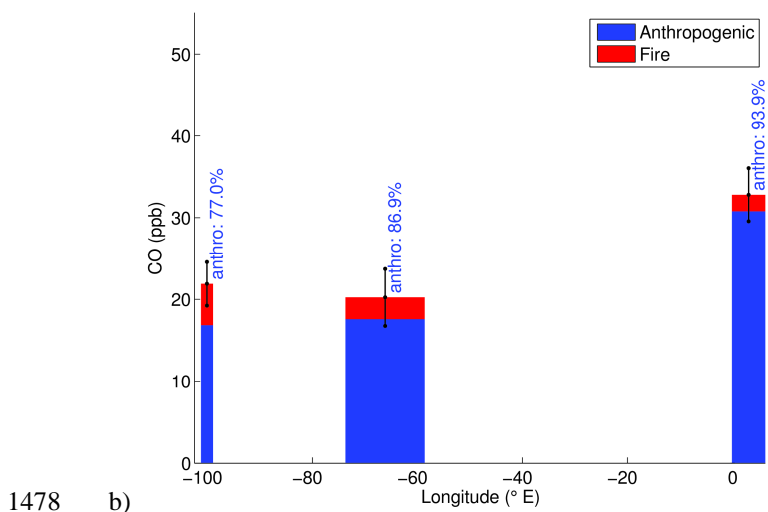
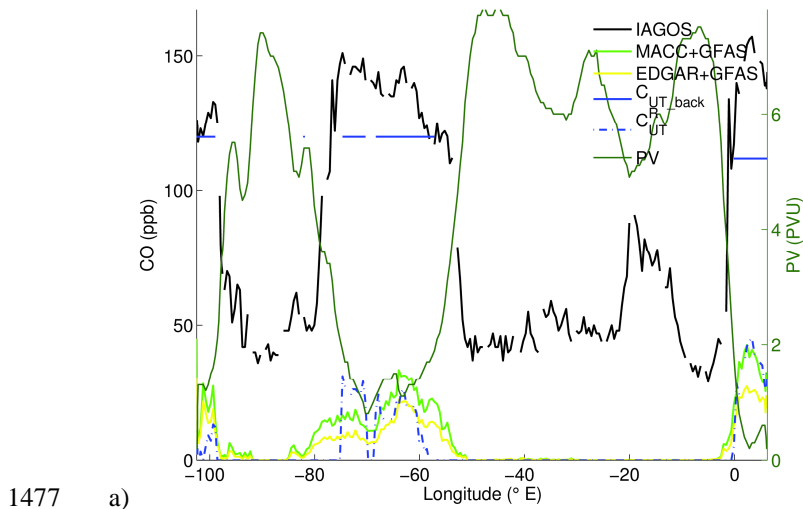
1466 b)



1467 c)

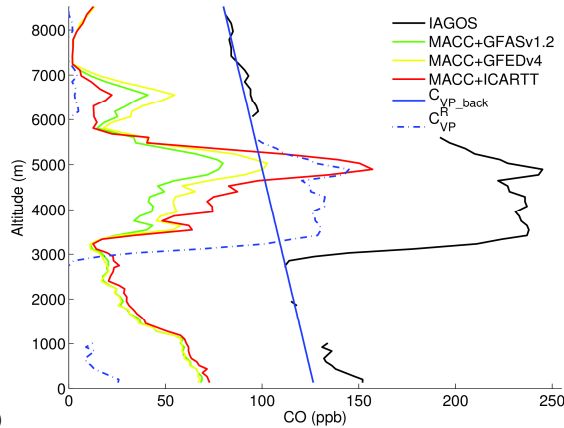
1468 **Figure 5: (a) Carbon monoxide profiles over Hong Kong during a MOZAIC-IAGOS flight landing on 22 October**
 1469 **2005. The black line indicates the observed CO profile while the blue line indicates the CO background deduced from**
 1470 **the observations. Green and yellow lines indicate the simulated CO contributions using respectively MACCcity and**
 1471 **EDGARv4.2 for anthropogenic emissions, and using GFAS v1.2 for biomass burning emissions. Simulated CO is**
 1472 **separated in (b) sources contribution (anthropogenic in blue, fires in red, standard deviation in black) and in (c)**
 1473 **regional anthropogenic origins (14 regions defined for global emission inventory,**
 1474 **<http://www.globalfiredata.org/data.html>, see Fig. S1; unshaded red square is for fire contribution), using MACCcity**
 1475 **and GFASv1.2.**

1476

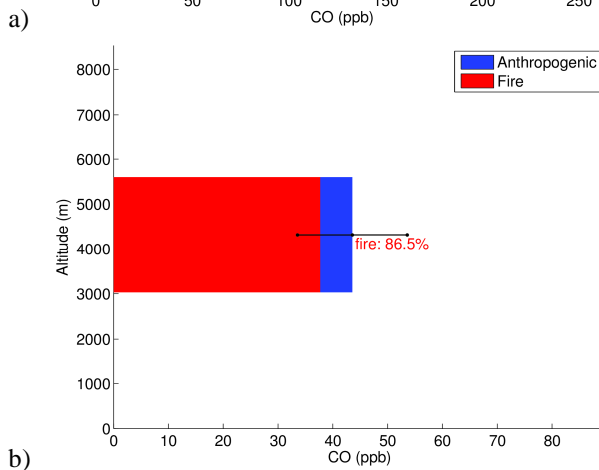


1480 **Figure 6: (a) Carbon monoxide zonal profile during the 10 March 2002 MOZAIC-IAGOS flight from Frankfurt to**
 1481 **Denver.** The black line indicates the observed CO while the blue line indicates CO seasonal background in the UT
 1482 deduced from the IAGOS data set. Light green and yellow lines indicate the simulated contributions using
 1483 respectively MACC and EDGARv4.2 for anthropogenic emissions, and GFAS v1.0 for biomass burning emissions.
 1484 Dark green represents potential vorticity (pvu) from ECMWF analyses. Simulated CO is separated in (b) sources
 1485 contribution (anthropogenic in blue, fires in red, standard deviation in black) and in (c) regional anthropogenic
 1486 origins (14 regions defined for global emission inventory, <http://www.globalfiredata.org/data.html>, see Fig. S1;
 1487 unshaded red square is for fire contribution), using MACCity and GFASv1.0.

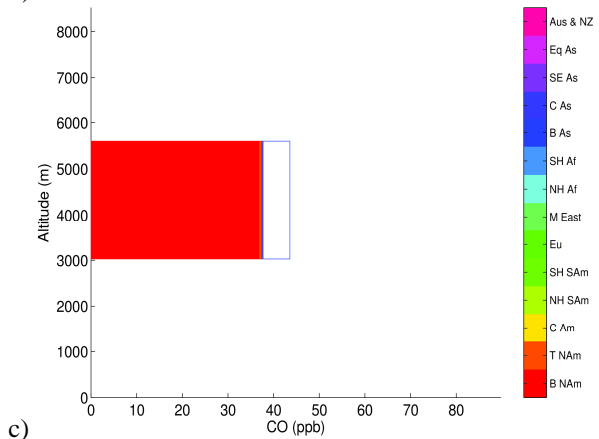
1488
 1489
 1490
 1491
 1492
 1493



1494



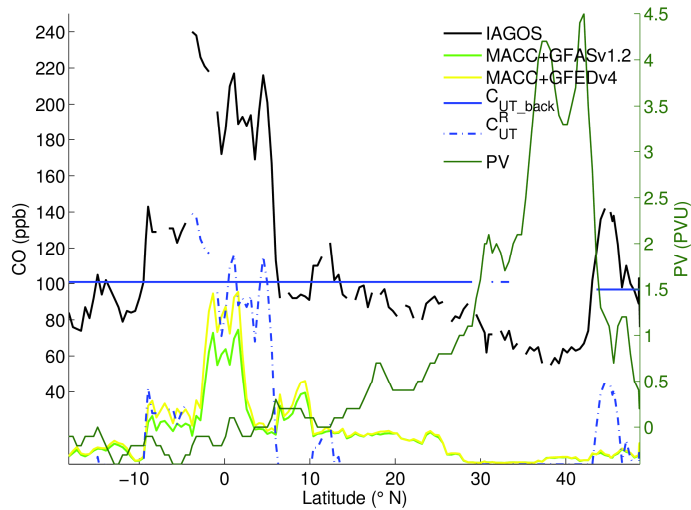
1495



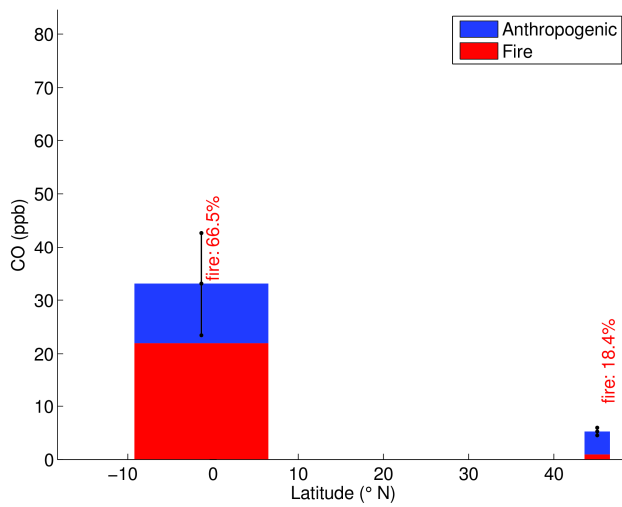
1496

Figure 7 : (a) Carbon monoxide profiles over Paris during a MOZAIC-IAGOS flight landing on 22 July 2004. The black line indicates the observed CO profile and the blue line indicates CO background deduced from the observations. Green, yellow and red lines indicate the simulated contributions using respectively GFASv1.2, GFED4 and ICARTT for biomass burning emissions, with MACCity for anthropogenic emissions. Simulated CO is separated in (b) sources contribution (anthropogenic in blue, fires in red, standard deviation in black) and in (c) regional biomass burning origins (14 regions defined for global emission inventory, <http://www.globalfiredata.org/data.html> see Fig. S1; unshaded blue square is for anthropogenic contribution), using MACCity and GFASv1.2.

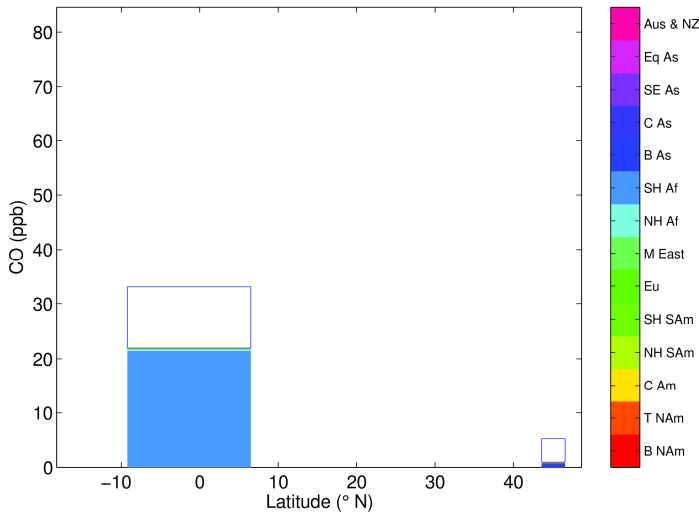
1504



1505 a)



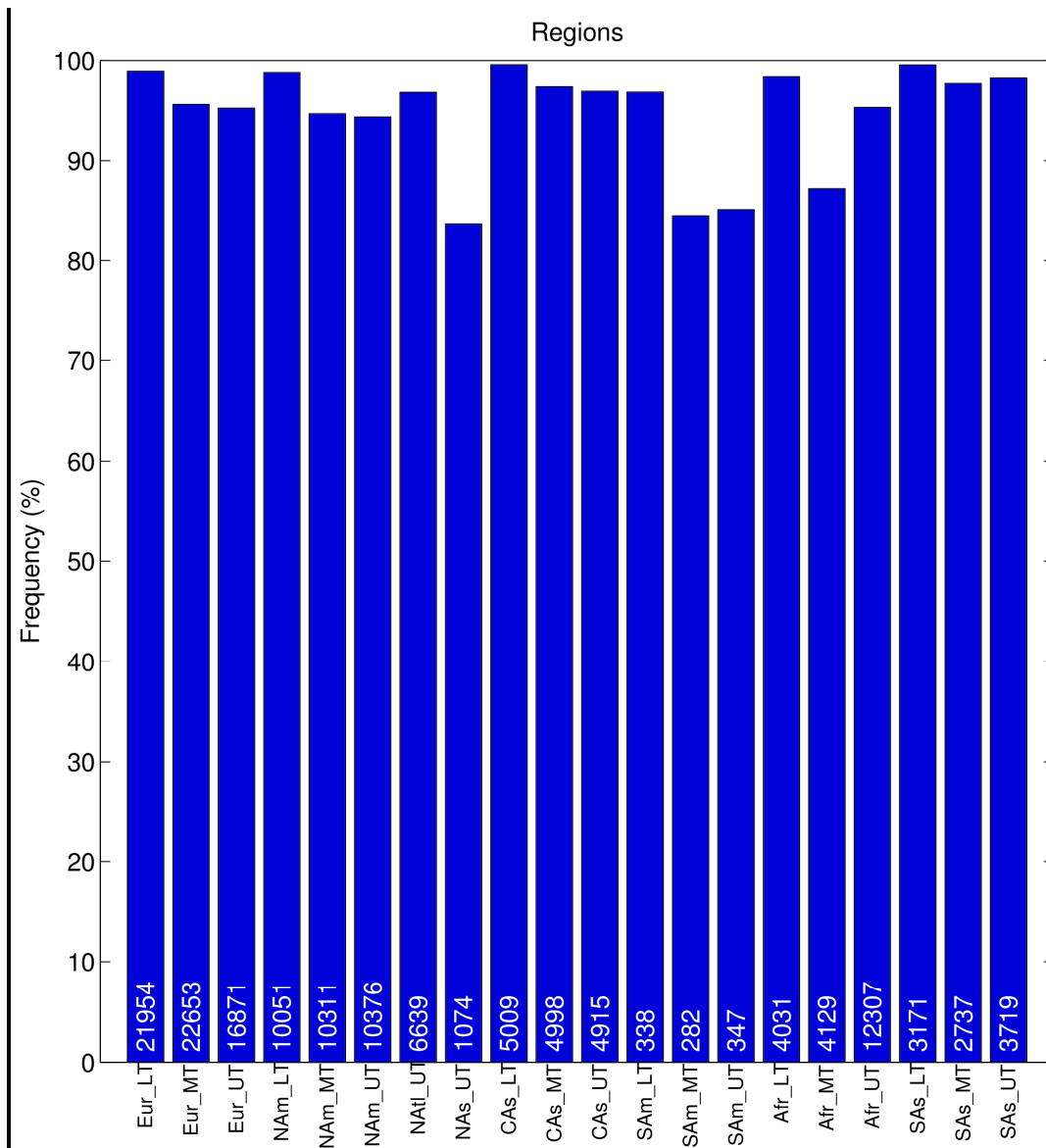
1506 b)



1507 c)

1508 **Figure 8:** (a) Carbon monoxide as a function of latitude during the 30 July 2008 MOZAIC-IAGOS flight from
 1509 Windhoek to Frankfurt. The black line indicates the observed CO, the blue line indicates the CO seasonal
 1510 background deduced from the IAGOS data set and the dash-dotted line the residual CO mixing ratio. Light green and
 1511 yellow lines indicate the simulated contributions using MACCity for anthropogenic emissions, and respectively GFAS
 1512 v1.2 and GFED4 for biomass burning emissions. Dark green represents potential vorticity (pvu) from ECMWF
 1513 analyses. Simulated CO is separated in (b) sources contribution (anthropogenic in blue, fires in red, standard
 1514 deviation in black) and in (c) regional biomass burning origins (14 regions defined for global emission inventory,
 1515 <http://www.globalfiredata.org/data.html>, see Fig. S1; unshaded blue square is for anthropogenic contribution), using
 1516 MACCity and GFASv1.2.

1517



1518

1519

1520

1521 **Figure 9: Frequency of plume detection (a) in different regions / altitudes / seasons using the MACCity and GFAS**
 1522 **v1.2 emission inventories during the 2003-2013 period. Biomass burning vertical injection uses APT methodology.**
 1523 **Altitude levels stand for LT=0-2km, MT=2-8km and UT=8km-tropopause. The numbers of the plumes observed in**
 1524 **each case are displayed in each box.**

1525

1526

1527

1528

1529

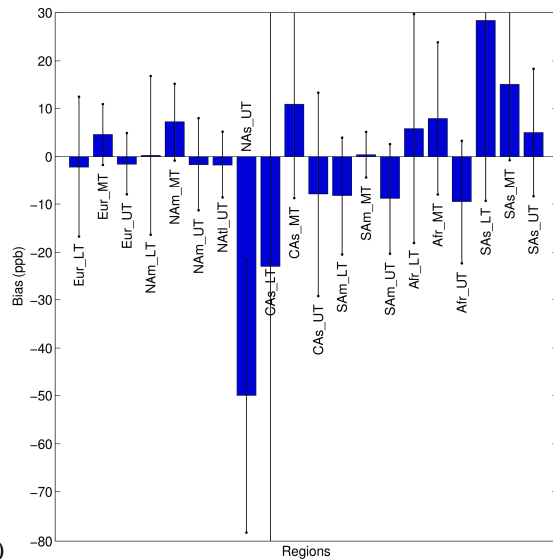
1530

1531

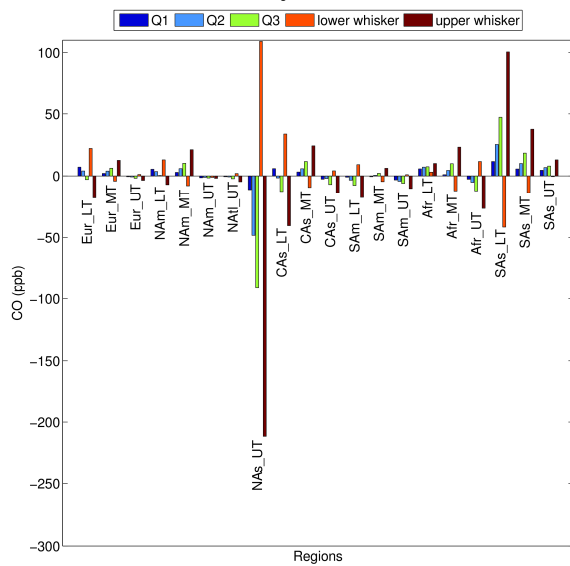
1532

1533

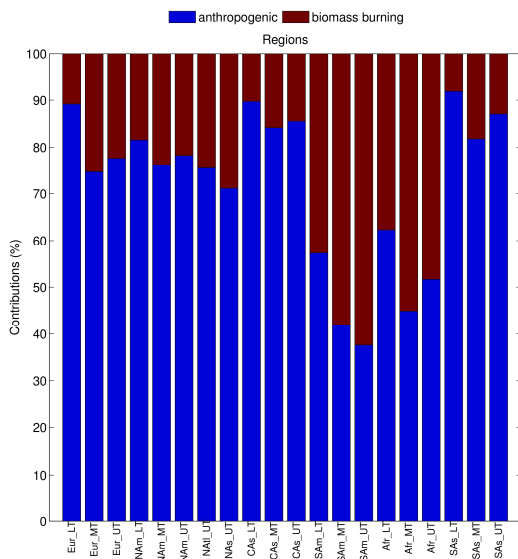
1534



1535 a)



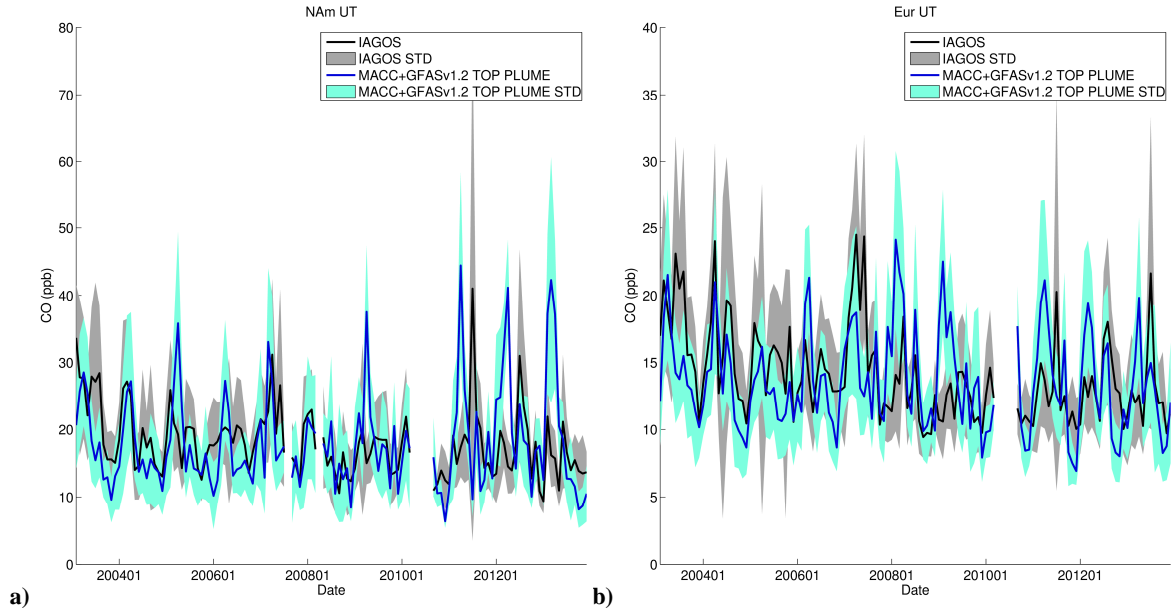
1536 b)



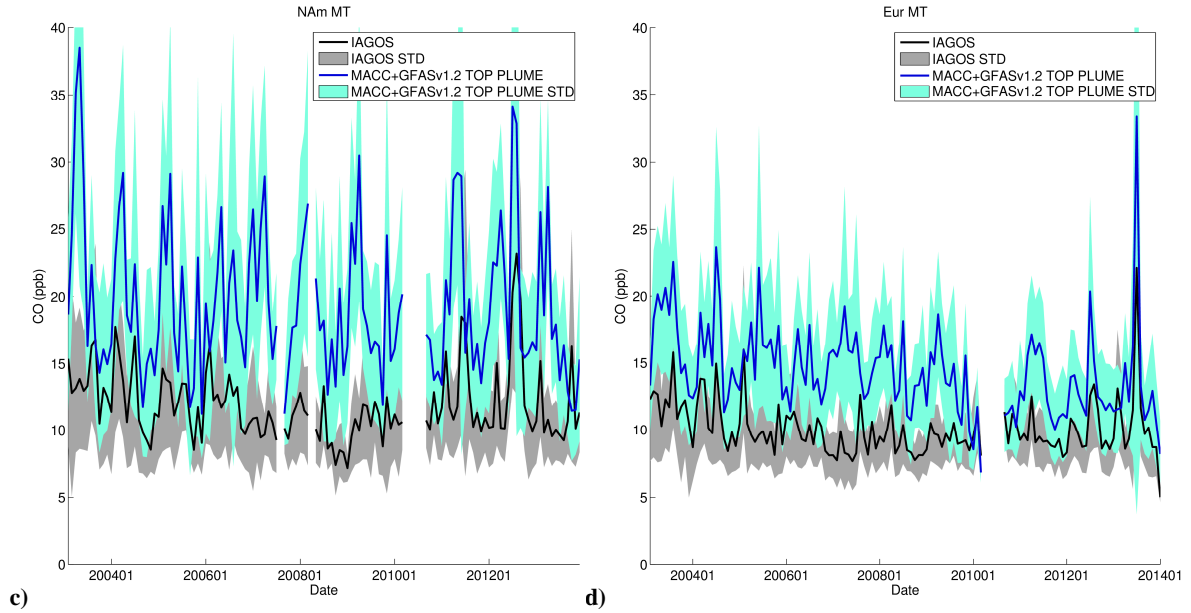
1537 c)

1538 **Figure 10: (a) Mean bias (blue) and mean standard deviation bias (black) between the modeled and observed CO**
 1539 **anomalies ; (b) Percentiles of the modeled CO anomalies bias with respect to observations; (c) Relative contribution**
 1540 **from anthropogenic and biomass burning sources to the modeled CO. The three graphs are for the main sampled**
 1541 **regions (Europe, North America, North Atlantic, North Asia, Central Asia, South America, Africa, South Asia) and in**
 1542 **three layers (LT, MT, UT), using MACCity and GFASv1.2 for the 2003-2013 period. Biomass burning vertical**
 1543 **injection uses APT methodology.**

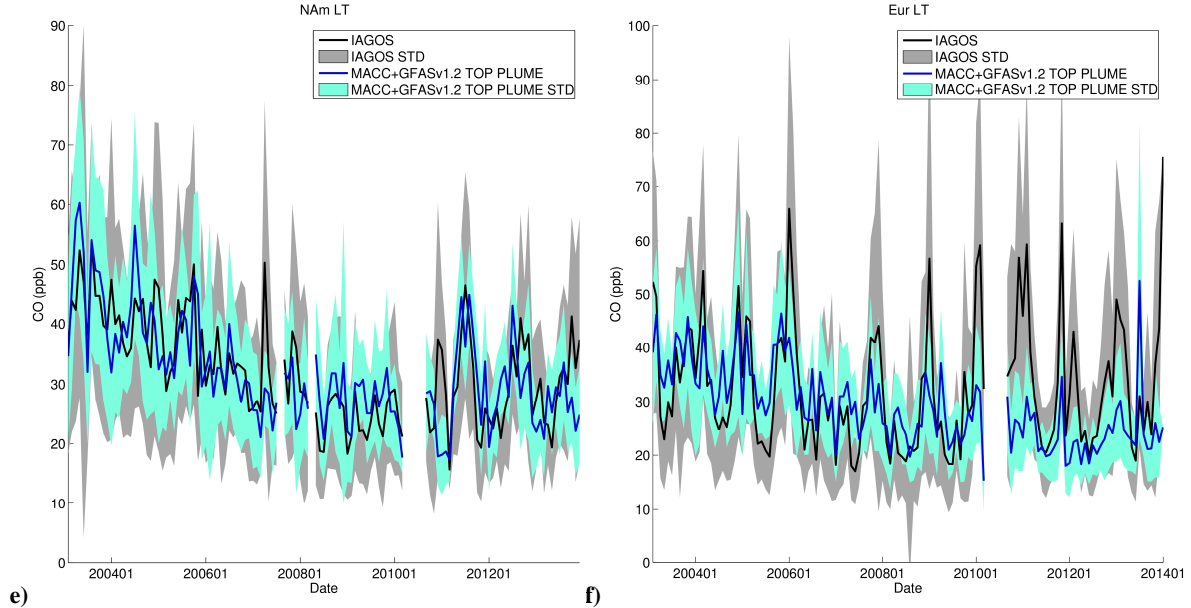
1544



1545



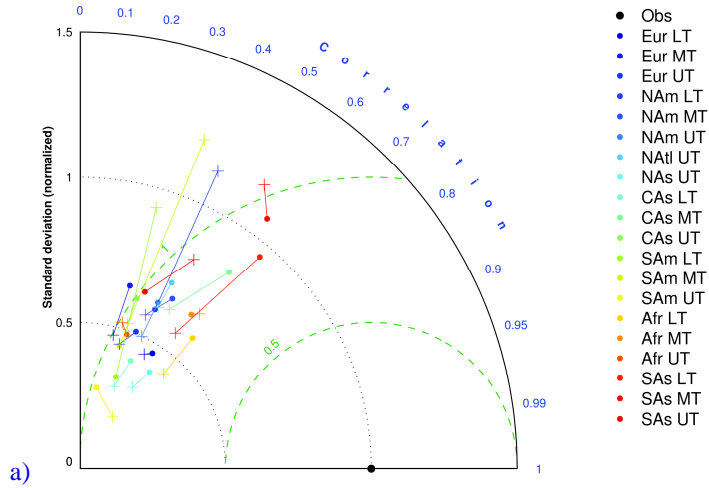
1546



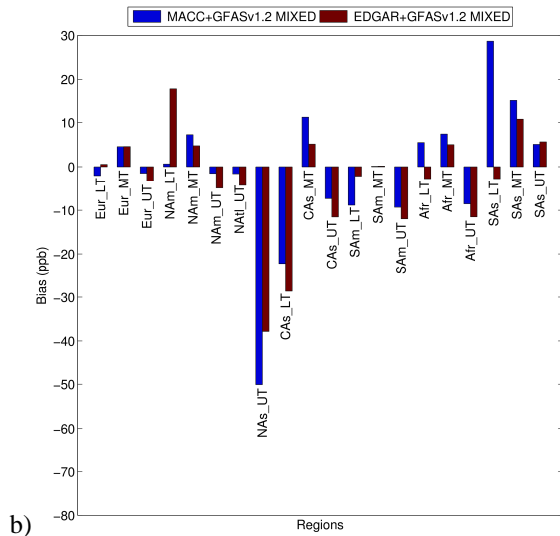
1547 **Figure 11: Times series (monthly means between 2003 and 2013) of the observed (black) and simulated (blue) plumes**
1548 **of CO enhancements for the two most documented regions (North America and Europe) in the LT (e & f), MT (c & d)**
1549 **and UT (a & b), using MACCity and GFASv1.2. Standard deviations are in gray (observations) and light blue (SOFT-**
1550 **IO). Biomass burning vertical injection uses APT methodology.**

1551
1552
1553
1554
1555
1556
1557
1558
1559
1560
1561
1562
1563
1564
1565
1566
1567
1568
1569
1570
1571
1572
1573
1574
1575
1576

1577



1578



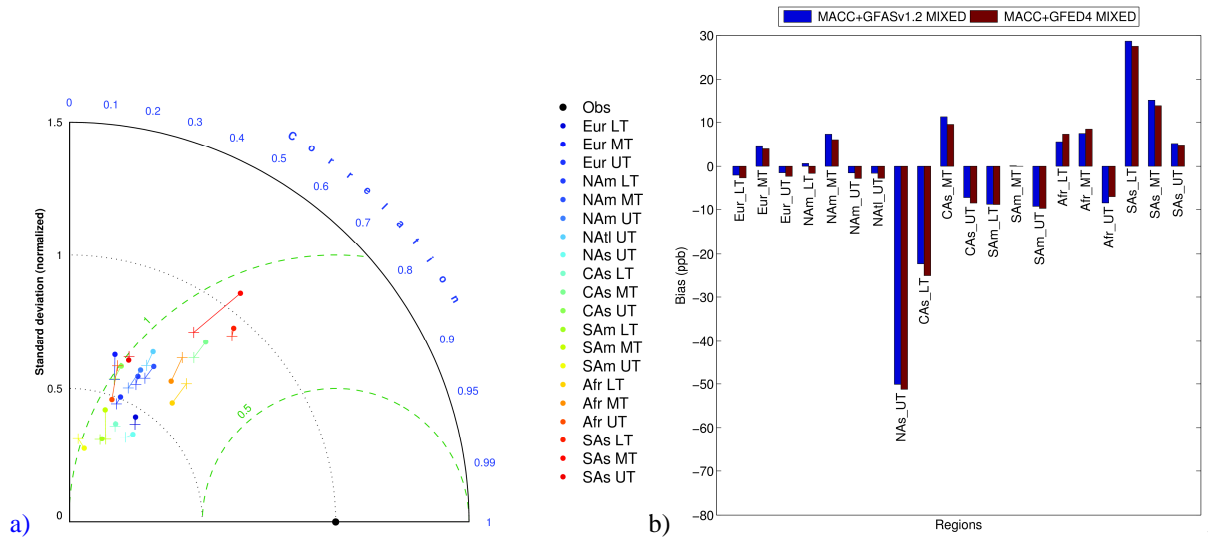
1579

1580

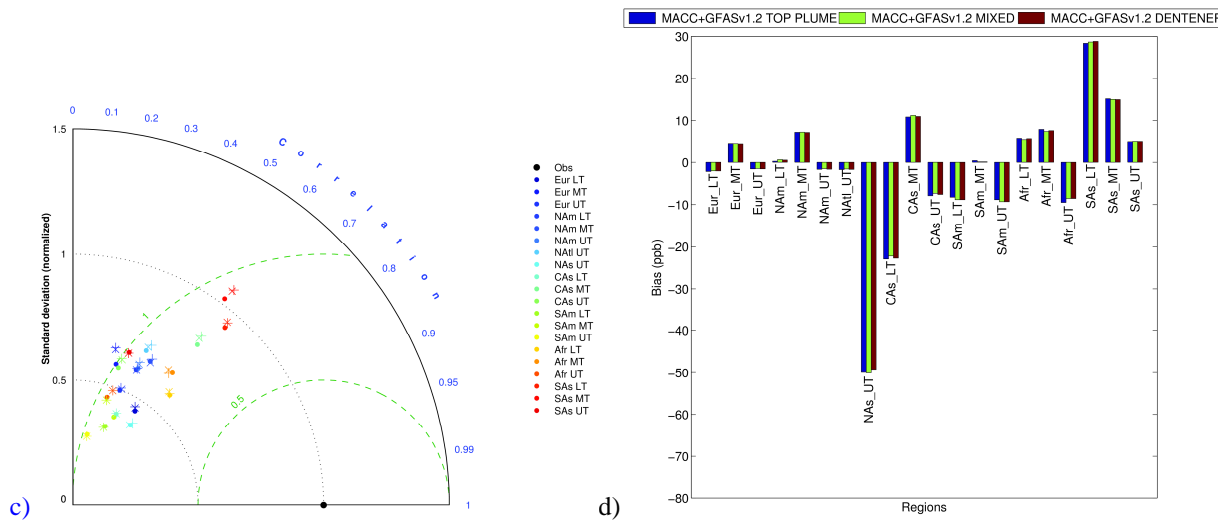
1581 **Figure 12: Comparison of the SOFT-IO anthropogenic emission influence between 2002 and 2008 (a) Taylor diagrams**
 1582 **are obtained for the different regions and in the three vertical layers (LT, MT and UT) using MACCcity (dots) and**
 1583 **EDGARv4.2 (crosses) with GFAS (lines represent connexions between the two inventories) (b) Mean biases between**
 1584 **the modelled (blue for MACCcity + GFAS; brown for EDGARv4.2 + GFAS) and observed CO anomalies. The MIXED**
 1585 **methodology is used for fire vertical injection**

1586

1587
1588



1589



1590

1591 **Figure 13: Comparison of the SOFT-IO biomass burning emission influence between 2003 and 2013. Taylor diagrams**
 1592 **are obtained for the different regions and in the three vertical layers (LT, MT and UT) using (a) GFASv1.2 (dots) and**
 1593 **GFED4 (crosses) with MACCcity and MIXED methodology for both GFASv1.2 and GFED4 (lines represent**
 1594 **connexions between the two inventories); (c) GFASv1.2 and MACCcity with different vertical fire injections**
 1595 **methodologies: MIXED (dots), APT (plus) and DENTENER (crosses) (lines represent connexions between the two**
 1596 **inventories). Mean biases between modeled and observed CO anomalies. Model is using (b) GFASv1.2 + MACCcity**
 1597 **(blue); GFED4 + MACCcity (brown) and MIXED methodology for both GFASv1.2 and GFED4; (d) GFASv1.2 +**
 1598 **MACCcity and different vertical fire injections methodologies: MIXED (blue); APT (green) and DENTENER (brown)**

1599

1600

1601

1602

1603

1604

1605